SEMMELWEIS EGYETEM

DOKTORI ISKOLA

Ph.D. értekezések

3339.

KOLLAI SAROLTA

Klinikai neurológiai kutatások

című program

Programvezető: Dr. Kovács Tibor, egyetemi tanár

Témavezető: Dr. Kovács Tibor, egyetemi tanár

TRANSNEURONAL DEGENERATION IN THE CENTRAL NERVOUS SYSTEM IN CEREBROVASCULAR DISEASES

PhD thesis

Sarolta Kollai

János Szentágothai Neurosciences Division

Semmelweis University

Supervisor:	Tibor Kovács, MD, Ph.D
Official reviewers:	Ferenc Nagy, MD, Ph.D
	Géza Szilágyi, MD, Ph.D
Head of the Complex Examination Committee:	János Réthelyi, MD, D.Sc
Members of the Complex Examination Committee:	Tibor Glasz, MD, Ph.D
	Magdolna Bokor, MD, Ph.D

Budapest

2025

TABLE OF CONTENTS

LIST OF ABBREVIATIONS

AH	anterior horn
AHC	anterior horn cell
ANOVA	analysis of variance
BBB	blood-brain barrier
CI	clustering index
CNS	central nervous system
CSF	cerebrospinal fluid
CST	corticospinal tract
CT	computed tomography
DAB	diamino-benzidin
DTI	diffusion tensor imaging
DWI	diffusion weighted imaging
EMG	electromyography
FA	fractional anisotropy
GFAP	glial fibrillary acidic protein
GDC	granular disintegration of the cytoskeleton
GLM	general linear model
HEM	hemorrhagic
Iba1	ionized calcium-binding adaptor molecule 1
ISC	ischemic
KB	Klüver-Barrera
LFB	Luxol fast blue
LGB	lateral geniculate body
MAG	myelin-associated glycoprotein
MAP	myelin associated protein
MBP	myelin basic protein
MCA	middle cerebral artery
MOG	myelin oligodendrocyte glycoprotein
MRI	magnetic resonance imaging
NF-H	neurofilament H

PCA	posterior cerebral artery
PLP	proteolipid protein
PNS	peripheral nervous system
ROS	reactive oxygen species
SpC	spinal cord
SYP	synaptophysin
TND	transneuronal degeneration
WD	Wallerian degeneration

1. INTRODUCTION

1.1. Secondary degeneration in the central nervous system

Secondary degeneration is a type of degeneration which is initiated by a primary neurological injury in structures remote from the primary lesion. Two types of secondary degeneration are distinguished: axonal degeneration and transneuronal degeneration (TND). (1, 2) Secondary axonal degeneration can be anterograde when it occurs distal to the lesion and retrograde when it is proximal to the lesion. In the former case, the anterograde axon degeneration is called as Wallerian degeneration (WD). (1)

TND can also be anterograde, when the cell innervated by the diseased neuron (i.e. the postsynaptic cell) degenerates secondarily, and retrograde, when the cell innervating the diseased cell (i.e. the presynaptic cell) is disease damaged or lost. (2)

In the followings, I will discuss WD and anterograd TND, as they are closely related to the present research.

1.1.1. Wallerian degeneration (WD)

Due to damage to the soma or disruption of the integrity of the axon, programmed degeneration of the distal part of the axon in a stereotyped manner is called WD. (3) The axon may be disrupted by complete rupture, compression/crushing, ischaemia or inflammation. The histopathological signs were first described by Augustus Volney Waller, a British electrophysiologist, in 1851, after cutting the tongue-innervating nerves of frogs, which in humans correspond to the hypoglossal and glossopharyngeal nerves. (4) This pathophysiological process has borne his name ever since and, although it can be observed both in the peripheral (PNS) and central nervous systems (CNS), it has different dynamics and morphological signs in the two sites. (5)

The original belief, lasting for a century and a half, that nutritional failure leads to degeneration was disproved with the discovery of the so-called slowWD (WldS) mice. (6) This is a strain of mice in which WD starts much later than in the wild type. It was concluded that WD is an active, programmed process, similar to apoptosis, the

mechanism of which is not fully understood, but has a set of time dependent molecular, cellular and morphological characteristics. (6-12) Of these, only the latter will be discussed in detail, considering the morphopathological topic of this work.

1.1.1.1. Morphological features of WD

WD involves four main events: axonal degeneration (axolysis), myelin breakdown (myelinolysis), debris clearance, and - in the case of peripheral nerves - Schwann cell proliferation and subsequent axonal regeneration. (13)

The first morphological feature of this process is the swelling of the axolemma (i.e. the axon membrane), during which the axon takes on a bead-like appearance. (5, 14) This process is known as granular disintegration of the cytoskeleton (GDC), and early ultrastructural sign of axonal degeneration, whereby the degradation of neurofilaments, microtubules and other components is initiated, resulting in the loss of conduction and fragmentation and the loss of axon structure. Electron micrographs reveal morphological similarities in degenerative features across both central and peripheral segments. (3, 5)

The spatiotemporal pattern (direction and speed) of axon degeneration is still under debate, but it is certainly influenced by a number of factors; type of injury (transection, crush, cell body death), species, age, fibre type, axonal diameter, anatomical localisation (PNS vs CNS) and environmental factors such as temperature. (3)

The structural changes in myelin begin concurrently with GDC and the fragmentation of axons. During this process, the myelin loses its continuity, becomes thinner in some places and swollen in others due to the loosening of the myelin lamellae, thus becoming irregular, and then, as the axon fragments, the myelin loses its continuity and forms egg-shaped myelin ovoids. (15-17)

The myelin ovoids detach from their associated glial cells - Schwann cells in the PNS, and oligodendrocytes in the CNS. This detached myelin parts are surrounded by astrocyte processes in the central nervous system. (3) This is followed by debris clearance performed by macrophages, some of which are resident microglia and some of which - if there is blood-brain barrier damage - are recruited from the monocyte-macrophage system from the periphery. (3, 18) The proportion of macrophages involved is determined by the

degree of blood-brain barrier damage, i.e. the primary lesion. Clearance proceeds more rapidly if peripheral macrophag recruitment is prominent. (3)

Following degeneration, oligodendrocytes may undergo atrophy, and the affected region will be gradually occupied by astrocytes forming glial scar. (19) In the peripheral nervous system, after Schwann cells dedifferentiate, they arrange themselves in a row within the lamina basalis, forming the so-called bands of Bunger. Thus, Schwann cells, their extensions and growth factors create a microenvironment that facilitates and guides axon regeneration. (20, 21)

Few human histological studies are available on the dynamics of corticospinal tract degeneration. In one study, the lateral corticospinal tract of patients who died after spinal cord injury was examined in a section a few cm distal to the injury. The time from injury to death ranged from 8 days to 1 year. Luxol staining showed myelin damage as early as 8 days post-injury, similarly Bielschowsky staining demonstrated axonal damage at day 8. (22)

Another comprehensive analysis after cerebral infarction examined the corticospinal tract in the cervical, thoracic and lumbar segments of the spinal cord. Axonal damage was detected by neurofilament immunohistochemistry in the cervical segment as early as day 12 post-stroke, whereas no such changes were seein in the thoracic and lumbar segments by the same time. (23)

Regarding myelin integrity, the same study examined MBP (myelin basic protein), a component of compact myelin, by immunohistochemistry. No abnormalities were found at day 14 post-stroke, but significant changes appeared by 5 weeks. (23) Another study from a similar sample specifically focused on the degradation of myelin proteins, investigated three additional three additional myelin associated proteins (MAPs): MAG (myelin-associated glycoprotein), located periaxonally, PLP (proteolipid protein) in compact myelin, MOG (myelin oligodendrocyte glycoprotein) located on the myelin surface. (24) Additionally immunohistochemical staining was used to monitor the neurite outgrowth inhibitor Nogo-A protein, produced by oligodendrocytes, which may play a role in inhibiting axonal regeneration in the CNS. Loss of MAG was first seen 14 days after stroke, the other proteins showed slow and gradual degradation. There are large gaps between cases in terms of the time between injury and death, so the onset of this is not

known, but from 5 weeks post-stroke a clear decrease is evident. MAG is no longer detectable after 10 months, whereas the other myelin proteins persisted in minimal amounts even 3 years later. (24)

In addition GFAP (glial fibrillary acidic protein), indicating astrocyte proliferation, was not detected until 6 months after injury in one study, while another study observed GFAP positivity 5 months post-injury. (22, 23)

1.1.1.2. WD in the CNS vs. in the PNS

WD differs between the CNS and PNS primarily in the ability for axonal regeneration. As for the time course of WD, the initial phases of degeneration proceed similarly in both systems. Axonal disintegration and myelin ovoid formation occur within similar time, however, clearance of myelin debris and ovoids is markedly slower in the CNS. In the periphery ovoids are rapidly cleared - 30 days in animal studies - and only myelin debris remains in place. In contrast, in the CNS, myelin ovoids and debris can persist for much longer, often remaining detectable for up to 90 days, and sometimes up to 250 days in animal studies. (5, 7, 25)

Since phases of the degeneration described above are prolonged in the CNS, many studies have suggested that this is the cause of the lack of regeneration, i.e. that the myelin proteins that remain there for a long time create an unfavourable environment for regeneration and inhibit it. (5) In conclusion, the reason for the lack of regeneration in the CNS is not clear, and although the slower degeneration, presumably due to the late appearance of macrophages, and the prolonged clearance of myelin structures seems a logical conclusion, the difference in the myelin sheath-forming cells (Schwann cell vs. oligodendrocyte) and their different behaviour may play the most important role. (5, 24, 26)

While slow axon regeneration takes place in the periphery, in the CNS, in the absence of regeneration, astrocytes fill in the place of the degraded tissue, forming a glial scar. (22, 25)

1.1.1.3. WD on MRI

In recent decades, imaging studies have made it possible to detect WD in vivo. Although the precise morphological changes underlying the various MR phenomena are not yet fully clarified, they are of great importance in establishing spatiotemporal dynamics, given that a subject can be examined successively at several time points. Previously, T2 sequences were only sensitive to the chronic phase, but with the emergence of DWI (diffusion weighted imaging) and DTI (diffusion tensor imaging), WD has become visible in the early phase. (22, 27, 28)

DWI-based studies are part of routine examination in neuroradiology, where the MR image is a quantitative image based on the diffusion rate of water molecules in the area under investigation. Diffusion refers to the random (Brownian) motion of water molecules. The rate of diffusion, in addition to being influenced by the molecule under investigation and the temperature, depends significantly on the microstructure of the environment; diffusion is highest in the cerebrospinal fluid (CSF) and more inhibited in the extracellular and intracellular spaces. This makes DWI measurements suitable for detecting early, mild structural changes in the nervous system. In ischaemia, changes in membrane permeability and cytotoxic oedema cause diffusion inhibition, andin Wallerian degeneration, secondary to neuronal dysfunction and glial proliferation, fluid volume and distribution are altered leading to restricted diffusion. (1, 28)

DTI is the most sensitive tool for detecting microstructural changes in white matter. Besides the degree of water diffusion, the diffusion tensor provides information on the preferred direction of water diffusion. In this case, the microstructure is determined by the integrity of the axon and myelin. (1) In DTI, the 3-dimensional shape of the diffusion motion is used to image the tissue. (29) In white matter, the movement of water is anisotropic, i.e. direction dependent, so that due to the structure of the axon membrane and myelin, water molecules move more easily and rapidly along the longitudinal direction of the fibers than perpendicular to them, the shape of the movement resembling a cigar. In contrast, in cerebrospinal fluid, for example, where the same movement is possible in all directions, the shape is spherical. (29)The degree of anisotropy depends accordingly on the integrity of the myelin and the axon, which decreases when the latter

is disrupted. The fractional anisotropy (FA) quantifies the anisotropy and can be set between 0 and 1, 0 for a spherical shape (isotropy) and 1 for an ellipse that is most different from a sphere (maximum anisotropy). (30) The mean diffusivity (MD) and the fractional anisotropy (FA) are indicators that quantify the amplitude and direction of movement of water molecules. (28, 31) The direction and magnitude of anisotropic diffusion can be used to reconstruct neural pathways, and a decrease in FA may indicate microstructural disruption or structural damage. (32)

1.1.1.4. MR signs of WD in the CNS after strokes

Acute-subacute stages of ischaemic stroke are only visible with DWI and DTI measurements. Summarizing the results of previous studies, after a complete middle cerebral artery (MCA) territory stroke, a decrease in FA value and DWI sign is seen in the corticospinal trract (CST) from day 7 onwards at the level of the pedunculus cerebri on the ipsilateral side, with some exceptional cases showing a difference earlier than this. There are fewer data from the level of the medulla oblongata, here the involvement of the CST is visible from the second week (days 4-10). (1, 33, 34) In hypertensive subcortical haemorrhage, similar dynamics were visible, so that the MR-sign of WD was seen in the first week (days 2-4-8) in the pedunculus, and in the second week, around day 14, in the medulla oblongata. (14, 27, 35-37)

T2-weighted scans show no difference until week 4, then between weeks 4 and 10 hyperintensity appears along the CST, presumably as a result of a transiently increased lipid-protein ratio due to myelin degradation. (38) From week 10-14 onwards, the CST becomes permanently hyperintense on T2-weighted images, presumably as a result of gliosis. (1)

According to an old classification of MR signs of WD, established by Kuhn in 1989, there are four stages of WD, based on T2-weighted imaging (39); I. no abnormality; II. hypointensity; III. hyperintensity; IV. atrophy. Currently, with the appearance of DWI and DTI, three stages are distinguished: acute (1-4 weeks), subacute (4-12 weeks) and chronic (after 12 weeks) (1). Kuhn's stage 4 is also visible on computed tomography (CT) scans. (40)

1.1.1.5. Early MR signs of WD and its relationship to clinical outcome

Several MRI studies have shown the prognostic role of early abnormalities indicative of WD, suggesting that early DWI or DTI abnormalities along the CST in both hemorrhagic and ischaemic strokes are associated with worse functional outcome. Its use may be helpful for early determination of rehabilitation potential, and may influence planned rehabilitation and care. (14, 27, 41-43)

1.1.2. Transneuronal degeneration (TND)

TND refers to secondary lesions in regions synaptically connected to the primary lesion. It is also referred to as transaxonal or transsynaptic degeneration. (2) It has been confirmed in many structures in the CNS by numerous animal and human experiments. (2)

Most human observations are from the the visual system, where multiple MRI investigations proved both anterograde and retrograde degeneration, also supported by histological studies in both forms. (44-49) After enucleation of an eye, optic nerve atrophy was observed. Over years, atrophy was seen in the region corresponding to the relay stations of the visual pathway, i.e. in layers 2, 3 and 5 of the ipsilateral lateral geniculate body (LGB) and layers 1, 4 and 6 of the contralateral LGB. .(45) Conversely, following occipital cortex damage, the entire ipsilateral LGB undergoes atrophy. (50-52)

In the limbic system, MR images have demonstrated signs of secondary degeneration in the mammillothalamic tract and ipsilateral mammillary body after temporal lobe epilepsy and posterior cerebral artery (PCA) infarction, respectively, and have also suggested secondary atrophy of the hippocampal formation after traumatic brain injury. (53, 54)

In the motor system, there are reports of secondary postischaemic involvement of the substantia nigra and globus pallidus after striatal infarction. (55, 56)

Secondary thalamic degeneration following MCA infarction has also been demonstrated in several studies. (57-59)

In addition, a remarkable histological case report demonstrated massive degeneration of the medulla oblongata and pons after many years of hemicerebellectomy. (60)

Crossed cerebellar atrophy is a contralateral middle cerebellar peduncle and contralateral cerebellar hemisphere atrophy following damage to the cortex or CST. (61, 62)

Hypertrophic olivary degeneration is a known form of transsynaptic degeneration caused by any kind of lesion in the Guillain-Mollaret triangle (dentatorubro-olivary pathway. If the synaptic connections to the inferior olive are disrupted, vacuoles and gliosis appear along with cell degeneration, giving it a hypertrophic appearance. (2, 63, 64)

1.1.2.1. TND in the spinal cord after stroke

Whether similar changes can occur in the spinal cord (SpC) is not yet clear: the results of previous animal studies are not consistent, although several have observed secondary degeneration of spinal motoneurons. (65-68) Human experiments have so far not yielded results of similar strength.

Only 2 human studies have dealt with this issue so far, one investigated the the anterior horn cells opposite to the lesion in the C5 segment 6 months or later after stroke; in this study, the mean cross-sectional area of anterior horn cells (AHCs) was significantly smaller compared to the opposite side, so they have pointed to some morphological change (69). Another study examined the L4 segment in only 4 cases and found no morphological differences 1-8 years after stroke. (70) This result is questioned by several methodological problems; on the one hand, the motoneurons of the segment under investigation are partially bilaterally innervated, which means that they do not completely lose their supranuclear connections, and on the other hand, the primary lesions were different - MCA territory stroke, 2 basal ganglia haemorrhages and a PCA territory infarct - not all of which are associated with CST involvement (PCA territory infarct).

1.1.2.2. Electrophysiological signs of secondary involvement of the SpC motoneurons

Until now, the strongest evidence for the secondary involvement of human spinal motoneurons after upper motoneuron damage has been provided by electrophysiological studies. When motor units are examined, there is a consistent finding that very early in the first week after stroke, and probably even on the first day, the number of functioning motor units is reduced. Of course, this does not indicate neuronal death at this early stage, but rather suggests a functional impairment, presumably caused by secondary transsynaptic damage to motoneurons due to loss of innervation from the upper motoneuron. (71-75)

Motor unit loss can be quantified using the MUNE (motor unit number estimation) method, which gives a numerical estimate of the number of functioning motoneurons. This estimation can be done by several methods, i.e. using different electrophysiological parameters. (72, 73, 76)

As a sign of denervation, spontaneous activity in the affected muscles can be detected with needle electrography within 2 weeks: fibrillation potentials or positive sharp waves appear and are recorded until the end of reinnervation, typically by the 6^{th} post-stroke month.

Loss of motor units is indicated by parameters indicative of reinnervation, such as polyphasic motor unit axon potential or jitter and clustering index (CI) determined by single-fibre electromyography. (75, 77, 78) In single-fiber EMG, the jitter, which is the variability of the latency of activation of muscle fibres, increases, which in this case, taking into account the underlying disease, is a sign of the re-forming of neuromuscular junctions, that is, reinnervation. (79) Also a sign of reinnervation is increased fibre density, which is the density of muscle fibres innervated by the same motoneuron. (78-80)

Likewise, reinnervation is indicated by an increased CI. A high CI indicates that the muscle fibres of a motor unit are located close together, i.e. one unit has more muscle fibres than usual. The measurement is based on fibre density and the estimated distance between fibres inferred from the waveform. (75, 81, 82)

Summarizing the electrophysiological phenomena, after stroke, paretic muscles show signs of denervation in the first 2 weeks, followed by a reduction in the number of functional motor units in the subsequent weeks. This decrease is first measured on day 9, increases for 3-4 months, and then stops. (73) Signs of reinnervation appear 4-6 weeks after the stroke, and reinnervation stops 6 months later. (77)

1.2. Microglia activation in the CNS

In the early 1900s, in addition to neurons and astrocytes, Cajal described a group of cells called the "3rd element" based on their poor staining. (83) Later, Hortega managed to stain and characterise these cells and divide them into two groups. One type of cell group was named microglia - the true "3rd element" in the CNS because of its mesodermal origin - and the other cell group was called oligodendroglia, which are closer to astrocytes because of their ectodermal origin. (84, 85)

Initially, microglia were considered to be part of the monocyte-macrophage system based on their phagocytic capacity, their morphological similarity to macrophages and their similar monocyte markers. (18)

Based on current knowledge, microglia are resident macrophages, immunocompetent cells found only in the CNS. They originate from progenitor cells of the corpus luteum, in contrast to peripheral macrophages, which arise from cells in the fetal liver and bone marrow. (84) Microglia are abundant in the CNS, accounting for 5-10% of all CNS cells. (83, 84, 86) Microglia are involved in the maintenance of homeostasis, in their activated state are an essential component of neuroinflammation and play an important role in the early development of the CNS. (87, 88)

In the fully developed CNS, in the resting state, by continuously stretching and retracting its processes, it is in active contact with all CNS components, "monitoring" its environment. This is referred to as the "resting" microglia, or more recently as the "homeostatic" glia, referring to its ongoing active function. (84, 86)

When needed, microglia change their function over a broad spectrum, i.e. they are activated. Microglial activation can involve several changes, depending on the

pathological process that inducing it, the involved CNS region and the age of the individual. (84) These include:

- amoeboid shape: at rest, microglia have a small soma and ramified processes; upon activation, the cell body enlarges, taking on an amoeboid shape with fewer and shorter processes
- migration
- phagocytosis
- release of bioactive substances: e.g.: cytokines, chemokines, reactive oxygen species (ROS) and neuroprotective factors. (18)
- altered protein markers: depending on the altered function, the expressed proteins change. (18, 84, 89) These proteins may be present at rest and change in abundance during activation, or they may be absent at rest and only appear during activation. By studying them, we can deduce the fact of microglial activation, which is the method we used in our studies. The most frequently studied proteins indicating microglial activation (18, 84, 90-92):
    - Iba1 (Ionized calcium-binding adaptor molecule 1): cytoplasmic protein, upregulated in inflammation. Involved in processes required for cell migration (such as cytoskeletal reorganization), and its presence is therefore a signal for migration and motility.
    - CD68: a lysosomal and endosomal transmembrane glycoprotein that signals phagocytic activation, which proved to be more sensitive than Iba1 for detecting acitvated microglia in subcortical white matter under pathological conditions. (93)
    - Human leukocyte antigen (HLA)-DR: MHC II cell surface receptor presenting antigen to immune cells, up-regulated in inflammation, expressed on the amoeboid form of microglia. (88)
    - Other possible proteins: MSR-A, CD64 P2Y12, CD115, CD11b, CX3CR1, MHCII, CD16, CD32, CD40, CD86, CD163, CD206. (84, 90)

Microglia is found in the CNS early in development, at the same time as neuronal development occurs, but before the appearance of astrocytes and oligodendroglia. Microglia plays an important role in several phases of neurodevelopment, regulating neurogenesis by controlling apoptosis and growth factor release, and later on it plays a role in neuronal plasticity and the development of neuronal networks. (18) Microglia also regulate the amount of synapses, by eliminating inactive synapses, a process known as synaptic pruning. (88)

Activated microglia are part of the process of neuroinflammation, which involves microglial activation, peripheral immune cell proliferation, cytokine and chemokine release and tissue injury (blood-brain barrier (BBB) injury, parenchymal injury). (84, 86) Neuroinflammation and thus microglial activation is partly beneficial because it tries to overcome the pathological process and partly harmful because it also causes tissue damage. (94, 95) Almost any pathological condition can trigger microglial activation. In the case of stroke, activation occurs within minutes at the site of tissue damage, followed by the opening of the BBB and the appearance of immune cells from the periphery in response to the cytokines released. (18) Activation has been observed not only at the site of primary damage, but also along the axon pathway and in synaptically connected areas such as the anterior horn of the SpC, in the lateral bundle of the SpC, and even in the thalamus, substantia nigra and hippocampus. (84, 94, 96)

In addition to the above, there are other conditions in which microglial function is not activated but is altered, such as chronic stress, ageing, or a bacterial or viral infection affecting other tissues outside the CNS. (84) Such impairment of microglial function is also known as “parainflammation” and may have long-term adverse consequences such as cognitive impairment or the development of neurodegenerative diseases. (90)

1.2.1. Microglial activation along the CST and in the SpC in vivo in human patients

In humans, microglial activation can be visualized by positron emission tomography imaging. This technique employs the radioligand 11C-PK11195, which binds to translocator protein — a mitochondrial membrane protein expressed exclusively by

activated microglia. Studies using this method have shown that microglial activation may persist from day 3 up to 6 months post-stroke along the CST. (97, 98)

In addition, a detailed human postmortem histopathological study examined microglial activation in the SpC of stroke patients. Using immunohistochemistry for MHC class II, leukocyte common antigen, and CD68, microglial activation was evident from day 3 post-stroke and remained detectable up to one year later both in the lateral column and the anterior horn of the cervical and thoracic spinal segments (98)

2. OBJECTIVES

The aim of our study was to map secondary degenerations of the CNS in cerebrovascular diseases. First, we investigated CST degeneration in patients with basal ganglia haemorrhage or total MCA territory stroke.

Since longitudinal histological analysis is not feasible, the temporal profile of WD in the CNS after stroke is not fully understood, the few histological findings available so far do not provide a complete description of the process and they hardly focus on the early period. Several MRI studies have confirmed the secondary degeneration of the CST, providing more information on the temporal dynamics, but the pathological substrate of MR phenomena with the pathological steps of WD is not yet fully clear.

In the first part of our work, we analysed the degeneration of the CST at the level of the pyramids in the medulla oblongata. Microglial activation was assessed by immunohistochemical detection of CD68 protein, structural lesions of the myelin were assessed by Klüver-Barrera staining (KB) for myelin, and NF-H neurofilament immunohistochemistry was used for the detection of axon degeneration.

Our aim was to gain a more detailed understanding of the pathological processes, especially in the early post-stroke period, and to compare the dynamics of the process in different stroke etiologies, i.e. haemorrhagic and ischaemic strokes.

Even less data are available regarding secondary degeneration of spinal motoneurons following upper motor neuron damage. TND in the SpC has not been definitely confirmed in human studies, and even experimental animal studies have yielded conflicting results. (14-17) Previous morphometric studies in human cases have focused on the chronic phase after cerebral infarction, whereas there are no histomorphological studies from the first month post-injury, although microglial activation is already evident in the anterior horn during this period and electrophysiological signs of functional damage to spinal motoneurons are clear from the first days following injury. (18-28)

Based on this, the aim of our research was to study the morphological and synaptic changes in the spinal anterior horn motoneurons. Morphometric examination of spinal

motoroneurons was performed post-mortem within one month after stroke using Nissl staining. In addition, we also detected microglial activation by CD68 immunohistochemistry and synapse density by synpatophysin (SYP) immunohistochemistry.

3. MATERIALS AND METHODS

3.1. Study population

For our analyses, histological samples were collected from patients died between 2002 and 2016 in the Department of Neurology, Semmelweis University.

For the first study, in which we investigated the degeneration of the CST in the medulla oblongata, 22 cases were studied. Statistical analysis was performed on 20 cases, with exclusion criteria being bilateral stroke or history of stroke or other CNS disease. Out of the 20 patients, 11 patients had extensive hemorrhagic stroke of hypertensive origin involving the internal capsule and 9 patients had ischemic stroke involving the entire MCA territory. All were confirmed by cranial CT in vivo and by post-mortem neuropathological examination. All patients had severe hemiparesis. (Table 1.)

The remaining 2 cases did not meet the above exclusion criteria and were not included in the statistical analysis, but nevertheless their histological analysis provided valuable information and were considered suitable for demonstration. One patient had bilateral strokes at 2 different time points, the other suffered a hemorrhagic stroke after a previous infarction more than 1 year before. (Table 1.)

In our second study, in which we analysed transsynaptic changes in the (SpC), seven patients were included for post-mortem analysis. Patients were adults over 18 years of age who had suffered a right or left total MCA territory infarction and had a maximum survival of 1 month after stroke. The complete MCA territory ischaemia was confirmed by CT and was also proven by post-mortem neuropathological examination. Patients with previous stroke or other CNS lesion in the medical history, with bilateral hemispheric infarction and with peripheral nerve injury of the upper limb were not included. Based on these criteria, the survival ranged from 3 to 32 days, the age of the subjects was between 73 and 85 years, and clinically all patients had severe hemiparesis. (Table 1.)

The study was approved by the Ethical Committee of the Semmelweis University, Budapest, Hungary (No. 79/2007).

Table 1. List of the patients included in the CST study and their clinical characteristics (H: hours; D: days)

patient ID	sex, age	type of stroke	side of the lesion	survival
1	M78	HEM	R	5H
2	M67	HEM	L	22H
3	M75	HEM	R	29H
4	F78	HEM	R	30H
5	F86	INF	L	2D
6	F80	INF	R	2D
7	M66	HEM	L	3D
8	M79	HEM	R	4D
9	F90	INF	R	5D
10	M77	HEM	R	7D
11	M65	HEM	R	10D
12	F82	INF	R	10D
13	F83	INF	L	11D
14	F73	HEM	L	17D
15	M64	HEM	L	18D
16	F90	INF	R	22D
17	M76	INF	R	27D
18	F60	INF	R	33D
19	M59	INF	R	42D
20	M52	HEM	R	90D
21	M62	INF	L	450D
22	M69	INF	L	330D

Table 2. List of the patients included in the SpC study and their clinical characteristics

Adapted from: *Early histopathological changes of secondary degeneration in the spinal cord after total MCA territory stroke*. Kollai S, Bereczki D, Glasz T, Hortobágyi T, Kovács T. Sci. Rep. 2023;13:21934. DOI:10.1038/s41598-023-49230-x. Licensed under CC BY 4.0.

	patients	sex, age	side of the infarct	survival (days)
D3	A	M74	R	3
	B	F81	R	3
	C	F85	R	3
D6-7	D	M73	R	6
	E	F79	L	7
D17	F	M80	R	17
D32	G	F85	R	32

3.2. Preparation of histological sections

Autopsies were performed within 48 hours of death. The brain and the SpC were removed and fixed in 10% formalin for 30 days. This was followed by neuropathological examination of the brains to confirm the total ischaemic involvement of the MCA territory or the haemorrhage involving the whole internal capsule and to exclude other pathology. Subsequently, the medulla oblongata at the level of the pyramid and/or the C6 segment of the SpC were prepared and embedded in paraffin and 10 μm thick sections were made.

From the spinal sections, to avoid overlap, every 6th section was Nissl stained (cresyl-violet, Reanal Labor, Budapest, Hungary), resulting in approximately 20 sections per case for morphometric measurements, the remaining sections were immunohistochemically stained, resulting in at least 3 additional CD68 (clone KP1, DAKO, Denmark; dilution 1:200) and 3 synaptophysin sections (clone DAK-SYNAP, Dako, Denmark; dilution of 1:200) per case. We used the VECTASTAIN Elite RTU kit (Vector Laboratories, USA) and as counterstaining hematoxylin was applied to aid morphological orientation.

Brainstem sections were taken from the lower part of the medulla oblongata above the decussation of the pyramid in cross-section. One KB (Luxol Fast Blue and cresyl violet; Reanal Labor, Budapest, Hungary) stained image from each case was analysed for myelin and two more were analysed for CD68 immunohistochemistry (clone KP1, DAKO, Denmark; dilution 1:200) and NF-H immunohistochemistry (clone N52.1.7, Leica Biosystems, USA; dilution 1:300) to assess microglia and axons, respectively.

3.3. The applied histological and immunohistological methods

Nissl staining (cresyl violet)

Nissl staining labels the ribosomes and endoplasmic reticulum within the soma of the neuron after fixation. Thus the nucleus will be blue and the endoplasmic reticulum in the plasma is purplish, the latter is also called Nissl material, or Nissl bodies. Since the axons remain unstained and the glial cells are not stained by the dye either, it is well suited for mapping the location, distribution and size of neurons and has therefore been used in our study for morphometric analysis of spinal motoneurons. (99)

Luxol Fast Blue

Luxol fast blue (LFB) binds to lipoproteins in myelin as a result of an acid-base reaction, during which a blue precipitate is formed. This makes it capable of detecting normal myelin, staining the white matter blue. Applied together with cresyl violet it is called Klüver-Barrera (KB) staining. With this combination, the neurons become visible and the myelin has a sharper contour. The absence of staining indicates damage or degradation of the myelin. (100, 101)

Immunohistochemistry

Immunohistochemistry involves the detection of a specific substance in a sample through an immunological reaction, i.e. antigen-antibody coupling. This coupling, however, is colorless and invisible and must be labeled for detection. In the case of immunohistochemistry, this labeling is done with an enzyme and a chromogenic substrate

bound to it. One of the most commonly used enzyme+substrate pairs is peroxidase and diaminobenzidine (DAB), which was used in our case, resulting in brown coloured reaction product. (102, 103)

CD68

There are several proteins expressed on microglial cells, some of which are found in resting microglia, others are expressed or increase in amount only during microglial activation, neuroinflammation. Examples of the latter include the cell surface receptor CD64 or HLA-DR, which play important role in antigen presentation and thus indication of immune response; Iba-1, which is upregulated in microglial migration and is marker of cell motility, and CD68, a lysosomal and endosomal transmembrane glycoprotein that is up-regulated in phagocytic activation. (18, 84) Since phagocytosis must be involved in the transneural and WD we studied, we chosed immunohistochemical detection of the CD68 molecule as the method of microglia detection.

Synaptophysin (SYP)

At the presynaptic terminal, neurotransmitters are stored in synaptic vesicles and released from there after fusion with the cell membrane. These vesicles from the presynaptic terminal contain a membrane protein called SYP. Its function is unkonwn, but since it can be found only in presynaptic terminals and is not present on the cell membrane or in other cell organelles, it is an excellent tool for studying the distribution of synapses. (104-106) By quantifying SYP using immunohistochemistry, we attempted to estimate the density of synapses in the entire anterior horn and on the surface of individual motoneurons.

Neurofilament (NF-H)

Neurofilaments are intermediate filaments according to their size, occurring exclusively in neurons and together with microtubules and microfilaments form the cytoskeleton of neurons. They consist of four subunits: the heavy (NF-H), medium (NF-M), and light (NF-L) chains, as well as internexin (Int). (107) In terms of their function, in addition to

providing the internal framework of the axon, they also determine the thickness of the axon, which influences the speed of conduction. (107) Since NFs within the cell are mainly located longitudinally in the axons, while they are less abundant in the dendrites and perikarions, their immunohistochemical detection can provide a good overall picture of axon distribution and integrity. (108, 109) This technique was applied in our study, during which NF-H was labeled.

3.4. Image analysis of the sections

In all cases, measurements were performed on both sides, the intact side was considered the control, and the abnormal side was compared to the control. Most of the axons of the CST cross in the lower level of the medulla oblongata, so in the case of the SpC we considered the side corresponding to the hemispheric infarct (ipsilesional) as intact and the opposite side (contralesional) as pathologic. (110) Conversely in the CST study, since the sections were taken above the level of the decussation, the SpC located on the side identical (ipsilesional) to the infarct/haemorraghe was considered pathologic and the opposite side (contralesional) intact. In the rest of this essay, we will use the terms intact (nonpathological - NPAT) and pathological (PAT) for simplicity and easier understanding.

The microscopic images were taken with a Zeiss Axio Imager M2 light microscope attached to a Zeiss Axiocam 503 color digital camera and a computer. Morphometric measurements of the SpC were performed on images taken at 40x magnification. The immunohistochemichal analysis of the SpC was made at 100x magnification. For brainstem sections, immunohistochemical analysis was performed at 200x magnification and myelin analysis at 600x magnification. SpC motoneuron size and microglia density measurements were performed for both SpC and brainstem by ZEN 2.6 computer software (Carl Zeiss AG, Germany). In the CST, the morphological changes of axons and myelin were assessed by inspection as at this early stage, swelling and irregular distribution of axons did not allow for their quantification.

3.4.1. Morphometric analysis of the SpC AHCs

In Nissl stained slices of SpC samples, in addition to the total number of AHCs, we measured the diameter, circumference and cross-sectional area of the AHCs. Cells with an area greater than 50 μm² and with clearly visible nucleoli located in the anterior horn were considered AHCs and included in the measurement. The anterior horn was defined as that part of the spinal grey matter that is bounded by a line that is laid on the ventral sulcus and another line perpendicular to it that runs through the central canal.

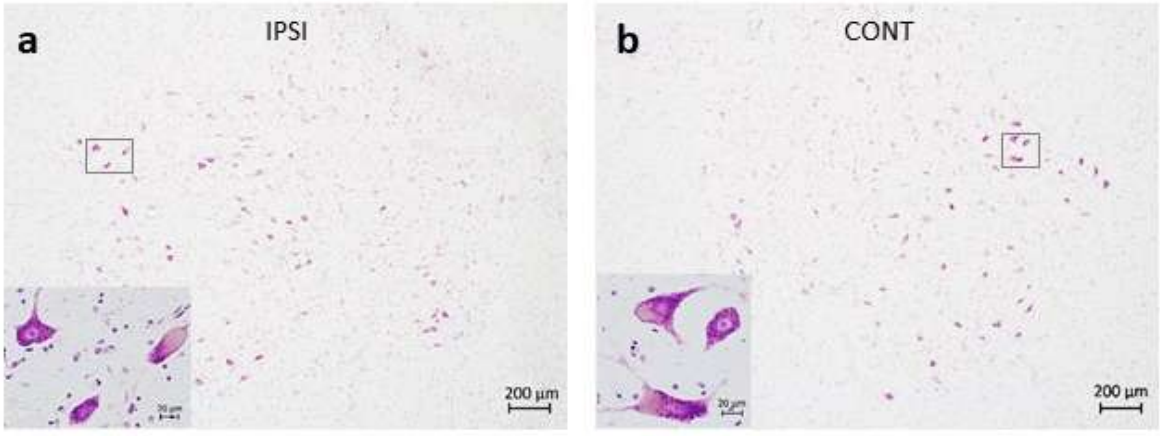

Figure 1. a, b AH-s on the intact (IPSI) **(a)** and on the contralesional (CONT) **(b)** side of the SpC. Large motoneurons are shown by the inserts. Nissl staining.

Adapted from: *Early histopathological changes of secondary degeneration in the spinal cord after total MCA territory stroke.* Kollai S, Bereczki D, Glasz T, Hortobágyi T, Kovács T. Sci. Rep. 2023;13:21934. DOI:10.1038/s41598-023-49230-x. Licensed under CC BY 4.0.

3.4.2. Analysis of microglia activation

As indicated above, microglial activation was judged by the presence of CD68-positive cells, which were visualized as brown dots on the sections by immunohistochemical labeling. Quantitative analysis of microglia was characterized by the density of CD68-positive cells, i.e. their total area divided by the area of interest.

For the SpC, we calculated density in the entire anterior horn determined by the method described above, in the lateral bundle in a circular area (with a radius of 690 μm), which we defined arbitrarily, and in the Rexed IX zone. The Rexed zone, also known as lamina

IX, contains the large motoneurons, and its localization was given by the connecting line laid on the large cells above 30 um in the anterior horn of the SpC.

In the brainstem sections after defining the pyramids by their anatomic localization, the CD68 density was calculated by the same way as mentioned above following manual substraction of macrophages, with measurements performed in an area of 4–8 mm^2.

3.4.3. Analysis of synaptic density

Synapse density was determined by measuring the SYP vesicle membrane protein density in the entire ventral horn and in the lamina IX using immunohistochemistry. These areas were determined according to the method described above. In addition, the SYP coverage of some large AHCs with an area above 30 μm^2 was measured, i.e. the SYP-covered area of the AHC was divided by the total perimeter of the AHC; 10-15 cells of each case were examined on both sides.

3.4.4. Inspection of the myelin and axonal structure in the brainstem

Due to swelling and dysintegration of the axons in the acute phase, we could not find a parameter to objectify and quantify the extent of axon degeneration and myelin loss for the NF-H and KB stained images. We evaluated these sections by inspection, the homogeneity of staining, axon arrangement, size distribution and spatial density of the NF-H stained sections were the criteria of interest. In KB-stained sections, myelin sheath surface, shape and myelin ring completeness - the proportion of the stained and non-stained areas - were assessed. In the very late cases staining intensity was evaluated by overview at low magnification and macroscopic examination.

3.4.5. Statistical analysis of the SpC data

The morphometric data were processed in three ways. First, ANOVA was used to compare the distribution of cell size in the two anterior horns in each case. Then, we performed a pooled analysis of the cases based on the number of days since the cerebral

infarction, in this latter case Mann-Whitney test was used. As a final part of our morphometric analysis, we divided the neurons into groups of large and small cells, and then compared the number of cells in each group with those in the opposite group using a Chi-squared test. We considered arbitrarily defined cells above 700 μm² as large cells and cells between 50 and 700 μm² as small cells.

The immunohistochemical results were evaluated together and the CD68 densities of the two (ipsilateral and contralateral) anterior horns, the lateral bundle and the Rexed zone were compared by t-test. Subsequently, CD68 densities of the total AH and the Rexed zone on the same side were compared by Sign and Wilcoxon tests in each case.

For synapse density, we compared SYP density of the AH and Rexed zone between the two sides using a t-test. Similarly, a t-test was used when comparing SYP coverage of large motoneurons of the two sides.

3.4.6. Statistical analysis of the CST/brainstem data

From the brainstem study, CD68 density values were statistically processed. Distribution of continuous variables was checked by the Shapiro-Wilk test. For multivariate analysis we used mixed-effect regression models. Density values between the pathological and non-pathological sides were compared by Wilcoxon matched pairs test in the total group and separately in the ISC and HEM subgroups. Spearman rank order correlation was used to evaluate the relationship between density values and time elapsed from stroke separately on the pathological and non-pathological sides. Kruskal-Wallis ANOVA was used to compare CD68 density values among the four groups based on the time after stroke. To identify the independent predictors of CD68 density the mixed-effects regression was used with stroke type (ISC or HEM), side of the lesion and sex as categorical variables and time from stroke and age as continuous variables as possible predictors. The mixed-effects approach was necessary due to repeated measurements on both sides of the patients. Time from stroke was modelled non-linearly in the regression model. Models with quadratic, square root and reciprocal relationships were investigated and were evaluated visually and using Akaike and Bayesian information criteria. A

difference of $p < 0.05$ was considered statistically significant. TIBCO statistica v. 14.0 and R v. 4.4.1 (USA) was used for data analysis.

4. RESULTS

4.1. Morphological changes of the CST in the medulla oblongata

Day 1-2

CD68 density is considerable in the CSTs on both sides of the medulla oblongata, however the difference between the two sides is not yet apparent. The axonal structure and myelin sheaths are still intact. The microscopic anatomy is the same as on the intact, nonpathological (NPAT) side.

Day 3-7

On the ipsilesional (pathological) side, the CD68 density is increased on the third day (Fig. 2d), and more macrophages are detectable by D7 (Fig. 2g). On D7, in circumscribed areas of the ipsilesional pyramid, the axonal structure shows the first signs of disintegration on NF-H staining, with swollen axonal cross-sections (Fig 2h). In addition, at this time, early signs of myelin degradation also appear (Fig 2i).

Day 10-18

CD68 density difference between the two sides is still very striking (Fig 2j). The signs of axonal degeneration are obvious; the axons are swollen, their structures lose integrity thus disappearing the regular structural pattern in the ipsilesional medulla oblongata (Fig. 2k). The signs of myelin degradation are prominent in several places with KB staining; the myelin rings lose their regular roundness and appear broken in several places with KB stain (Fig. 2l).

After 1 month

Besides the continuing strong CD68 density difference (Fig. 2m) and the obvious signs of the ongoing axon degeneration (Fig. 2n), the signs of myelin degradation become more evident, i.e. decrease in staining intensity with only sparse visible myelin rings (Fig. 2o). The severity of the pathology remains similar after three months (not shown).

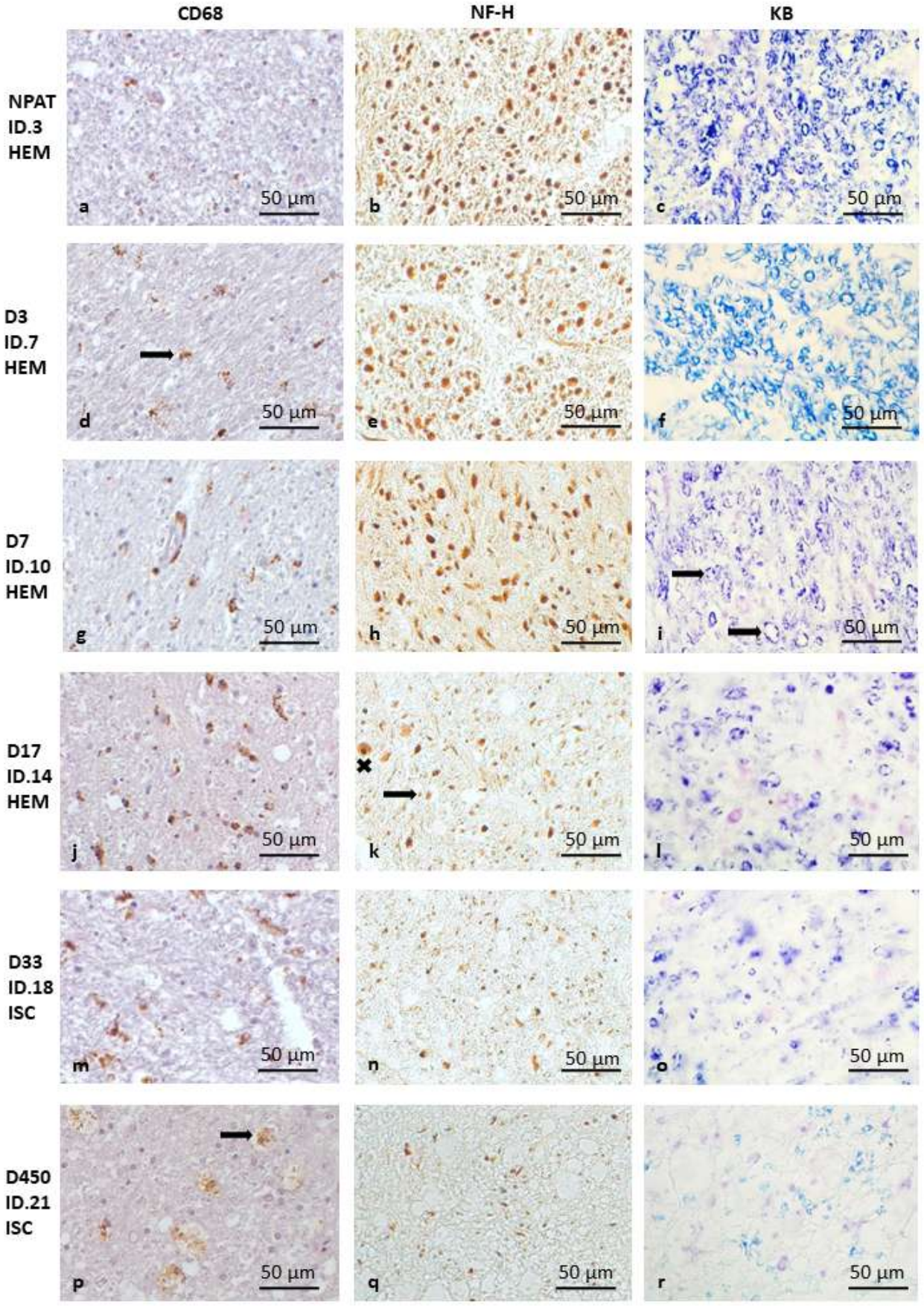
CD68
NF-H
KB
NPAT
ID.3
HEM
D3
ID.7
HEM
D7
ID.10
HEM
D17
ID.14
HEM
D33
ID.18
ISC
D450
ID.21
ISC
a
b
c
d
e
f
g
h
i
j
k
l
m
n
o
p
q
r
50 µm

Figure 2. Pathology of the CST degeneration in the pyramids of the medulla oblongata following HEM and ISC stroke (as the changes are similar, ISC and HEM cases are not shown separately). CD68 immunohistochemistry (a, d, g, j, m, p), NF-H immunohistochemistry (b, e, h, k, n, q) and Klüver-Barrera staining (c, f, i, l, o, r). The bar in the bottom right corner of the pictures indicates 50 μm. Intact (NPAT) side of the pyramid in the medulla oblongata (a, b, c) for comparison (D3 ISC). Very early HEM case (day 3 - D3) with microglial activation (d) (brown spots) (arrow shows a ramified microglia) but without signs of myelin (e) or axon degeneration (f). Early (day 7 -D7) HEM case with incipient axon and myelin destruction (arrows show breaking of the myelin rings) (g, h, i). Intermediate (day 17 - D17) (j, k, l) (HEM) and late (ISC) case (day 33- D33) (m, n, o) with marked myelin degradation (l, o), axon degeneration (k, n) (arrow shows a shrunken, while "x" shows a swollen axon) and increasing microglial activity (j, m). Very late stage of CST degeneration (D450 ISC) with several macrophages (arrow) and extensive loss of axons and myelin (p, q, r).

After 1 year

In the 2 additional late cases (D330 and D450), the number of CD68 positive cells are still significantly increased on the pathological side (Fig. 2p), with a high density of microglia together with macrophages along the surface of the medullary pyramid. Axon density is dramatically reduced, with the remaining fibers being thinner compared to the intact side (Fig. 2q). Myelin staining is significantly diminished, but signs of myelin degradation are still present (Fig. 2r).

4.2. Comparison of haemorrhagic and ischemic stroke cases

Comparing the HEM and ISC groups, the overall CD68 density on the ipsilesional side (HEM n = 11 (mean ± SD): 12515 ± 8127); (ISC n = 9 (mean± SD): 14871 ± 5639); (all cases n = 20 (mean ± SD): 13353 ± 6898) was approximately twice that on the contralesional side (HEM n = 11 (mean ± SD): 6937 ± 2151); (ISC n = 9 (mean ± SD):

7866 ± 3751); (all cases n = 20 (mean ± SD): 7436 ± 2898) in both patient groups (Wilcoxon matched pairs test p(all cases) = 0,0005), and no difference was observed between HEM and ISC when comparing the pathological sides (p = 0,4780).

When examining the whole group, considering time as a continuous variable, CD68 density on the ipsilesional side significantly correlated with survival time (Spearman Rank Order Correlations n = 20 p < 0.0001).

A similar result is obtained when four time points are formed; there is a significant difference in density between time groups on the ipsilesional side (Kruskal-Wallis ANOVA n = 20 p = 0.0047). No similar correlation was observed on the contralesional side.

Analysing HEM and ISC separately, density on the ipsilesional side is correlated with time elapsed in both patient groups, but no such correlation on the contralesional side could be proven (Spearman Rank Order Correlations HEM n = 11 p = 0.005; ISC n: 9 p = 0.013). By multivariate analysis using a mixed-effect regression model, independent predictors of CD68 density were survival time (p = 0.003 for the linear and p = 0.248 for the non-linear term), and side of lesion (ipsi- vs contralesional; p < 0.001) but not sex, age or stroke type. The relationship between CD68 and survival time density was modelled using a reciprocal curve, based on the visual assessment and information criteria. CD68 density is still increasing after 3 months of survival. (Fig. 3) Based on the long-survival time cases, the microglial activation is still present 1.5 years after the stroke.

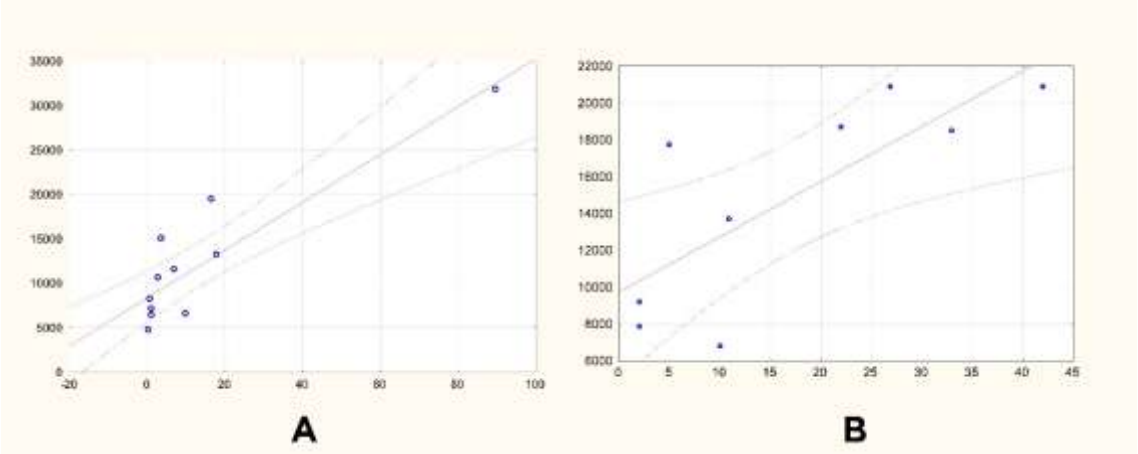

Figure 3. Changes in CD68 density in the ipsilesional pyramid of the medulla oblongata HEM (a) and ISC (b) groups are shown separately. Horizontal axis: survival in days; vertical axis: CD68 density in μm²/mm².

4.3. AHC morphometry

Morphometric data did not prove neuronal loss in the contralesional AH of the SpC in the first 30 days after the MCA infarction (p = 0,13). In the D3 cases, cells on the contralesional side were significantly smaller, while in the D6-7 cases, they were significantly larger in all three parameters. When the cases were evaluated individually, similar results were obtained, but the difference was significant only in the 6 and one of the 3 day cases (p = 0,00001, p = 0,00001, p = 0,00001 at 6 and p = 0,009061, p = 0,008247, p = 0,030579 at 3 days). In D17 and D32 patients, no significant difference was seen between the ipsi- and contralesional sides in these parameters (Table 3Fig. 5).

Table 3. Cell sizes in the AH according the age of the MCA infarct

Adapted from: *Early histopathological changes of secondary degeneration in the spinal cord after total MCA territory stroke.* Kollai S, Bereczki D, Glasz T, Hortobágyi T, Kovács T. *Sci. Rep.* 2023;13:21934. DOI:10.1038/s41598-023-49230-x. Licensed under CC BY 4.0.

	Cell number (n)		**Cross sectional area (µm²)**			**Diameter (µm)**			**Perimeter (µm)**		
	IPSI	CONT	IPSI	CONT	p	IPSI	CONT	p	IPSI	CONT	p
D3	3099	3142	403,9±292,8	388,3± 290,7	**0,006**	21,3±7,5	20,8±7,6	**0,006**	86,5±37,0	84,9±37,3	**0.006**
D6-7	1961	2125	366,8±287,4	416,9±335,879	**<0.001**	20,3±7,4	21,5±8,2	**<0.001**	80,2±34,3	85,4±38,3	**<0.001**
D17	1013	1044	332,8±207,1	342,9±200,574	0,103	19,6±6,0	20,0±5,9	0,103	80,9±32,2	82,8±30,9	**0,047**
D32	1154	1182	371,5±312,0	387,9±320,630	0,312	20,2±8,0	20,6±8,2	0,312	91,1±60,8	97,1±115,6	0,485

The proportion of large cells was significantly higher on the contralesional side in the D6-7 cases (D6: p = 0,0001 and D7: p = 0,0330), while no similar shift in the ratio of cell size was revealed in the earlier or later cases (Fig. 4).

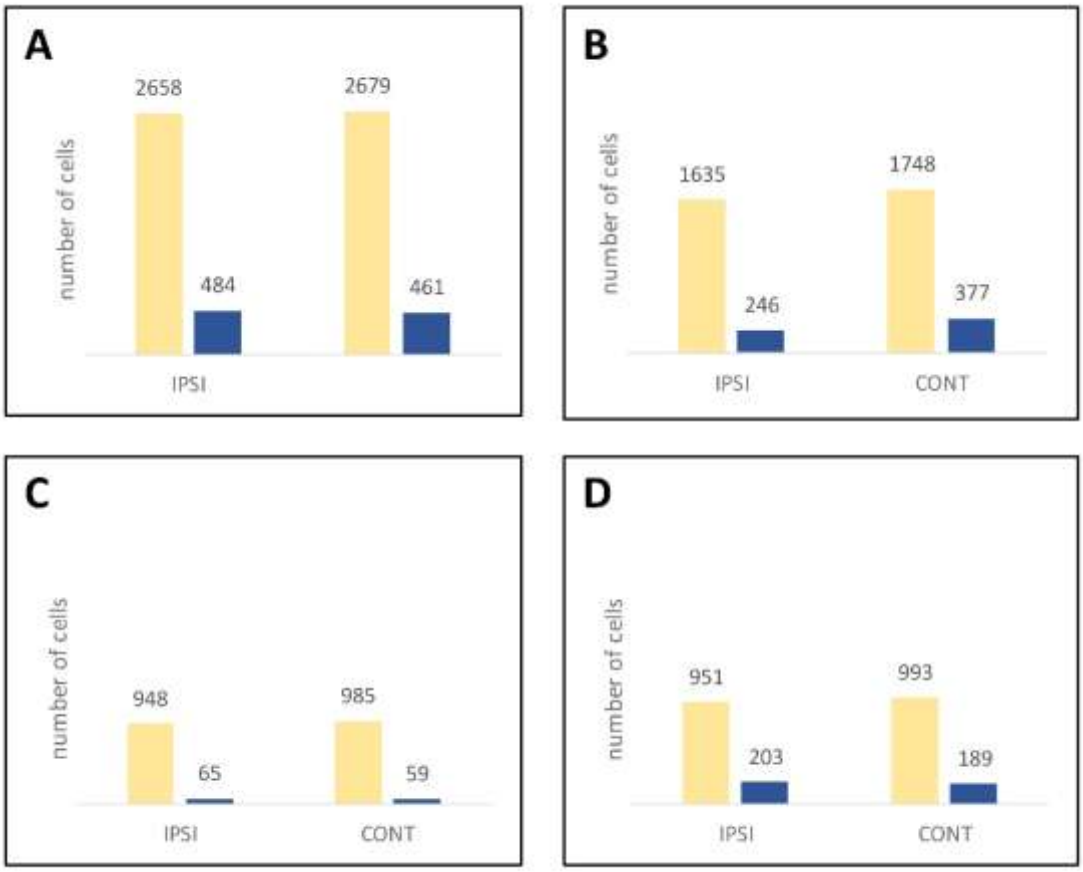

Figure 4. a, b, c, d Number of cells < 700 μm² (light color columns) and 700 um² <(dark color columns) on the intact (IPSI) and contralesional (CONT) side 3 **(a)**, 6-7 **(b)**, 17 **(c)** and 32 **(d)** days after total MCA territory stroke.

.

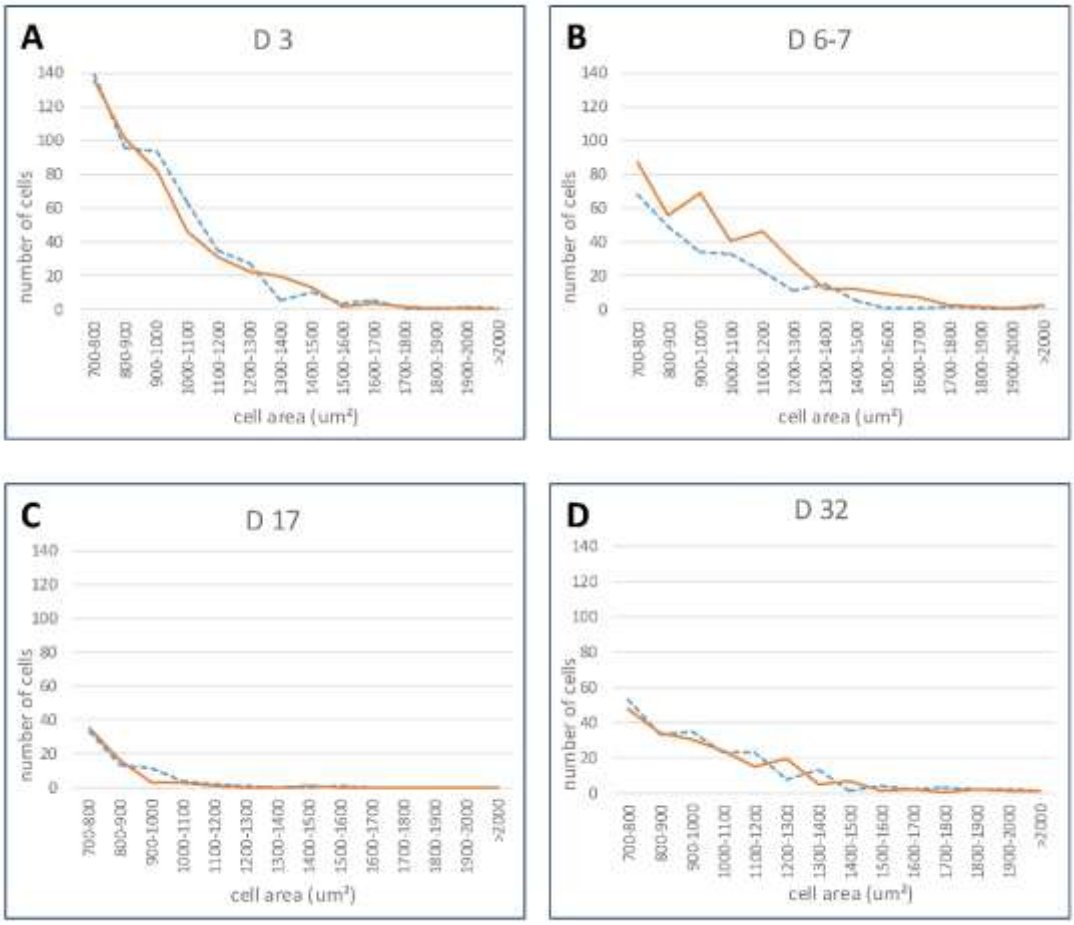

Figure 5. a, b, c, d Distribution of cells over 700 um² by cross sectional area (cell area) 3 **(a)**, 6-7 **(b)**, 17 **(c)** and 32 **(d)** days after total MCA territory stroke. Dotted line indicates the ipsilesional (IPSI), while continuous one is the contralesional (CONT) side.

Modified from *Early histopathological changes of secondary degeneration in the spinal cord after total MCA territory stroke*. Kollai S, Bereczki D, Glasz T, Hortobágyi T, Kovács T. Sci. Rep. 2023;13:21934. DOI:10.1038/s41598-023-49230-x. Licensed under CC BY 4.0.

4.4. Immunohistochemical morphometry of microglia in the AH

CD68 immunohistochemistry (Fig. 6 a, b, c, d) displayed an outstanding increase in density in the whole contralesional AH (ipsilesional side (mean ± SD): 0,0020 ± 0,0014, contralesional side (mean ± SD): 0,0039± 0,0024; n = 21; p = 0,0008), and this difference was seen already on the third day after MCA occlusion and did not disappear later on. On the contralesional side, CD68 density was higher in the Rexed's lamina IX compared

to the whole AH (CD68 density in Rexed's lamina IX: ipsilesional (mean ± SD): 0,0020 ± 0,0015; contralesional (mean ± SD): 0,0049 ± 0,0031); (Sign test: n = 21; p = 0,0088; Wilcoxon: n = 21; p = 0,0172), while similar distribution difference could not be observed on the ipsilesional side.

A similar remarkable difference was observed in the CD68 density in the CST in the lateral bundle on the contralesional side compared to the intact ipsilesional side (density ipsilesional (mean ± SD): 0,0024 ± 0,0016; contralesional (mean ± SD): 0,0058 ± 0,0034 p = 0,0008).

4.5. Immunohistochemical morphometry of synapses in the AH

SYP density (all cases) (Fig. 6 e, f) was identical on both sides in the complete AH and in the Rexed's lamina IX as well (SYP density ipsilesional side (mean ± SD): 0,2731 ± 0,0878; contralesional side (mean ± SD): 0,2683 ± 0,0870 n = 21, p = 0,4020), while the SYP coverage (all cases) of the individual motoneurons was significantly decreased on the contralesional side (SYP coverage ipsilesional: mean ± SD: 0,8341 ± 0,1298; contralesional: mean ± SD: 0,7557 ± 0,1499 n = 70 p = 0,0001).

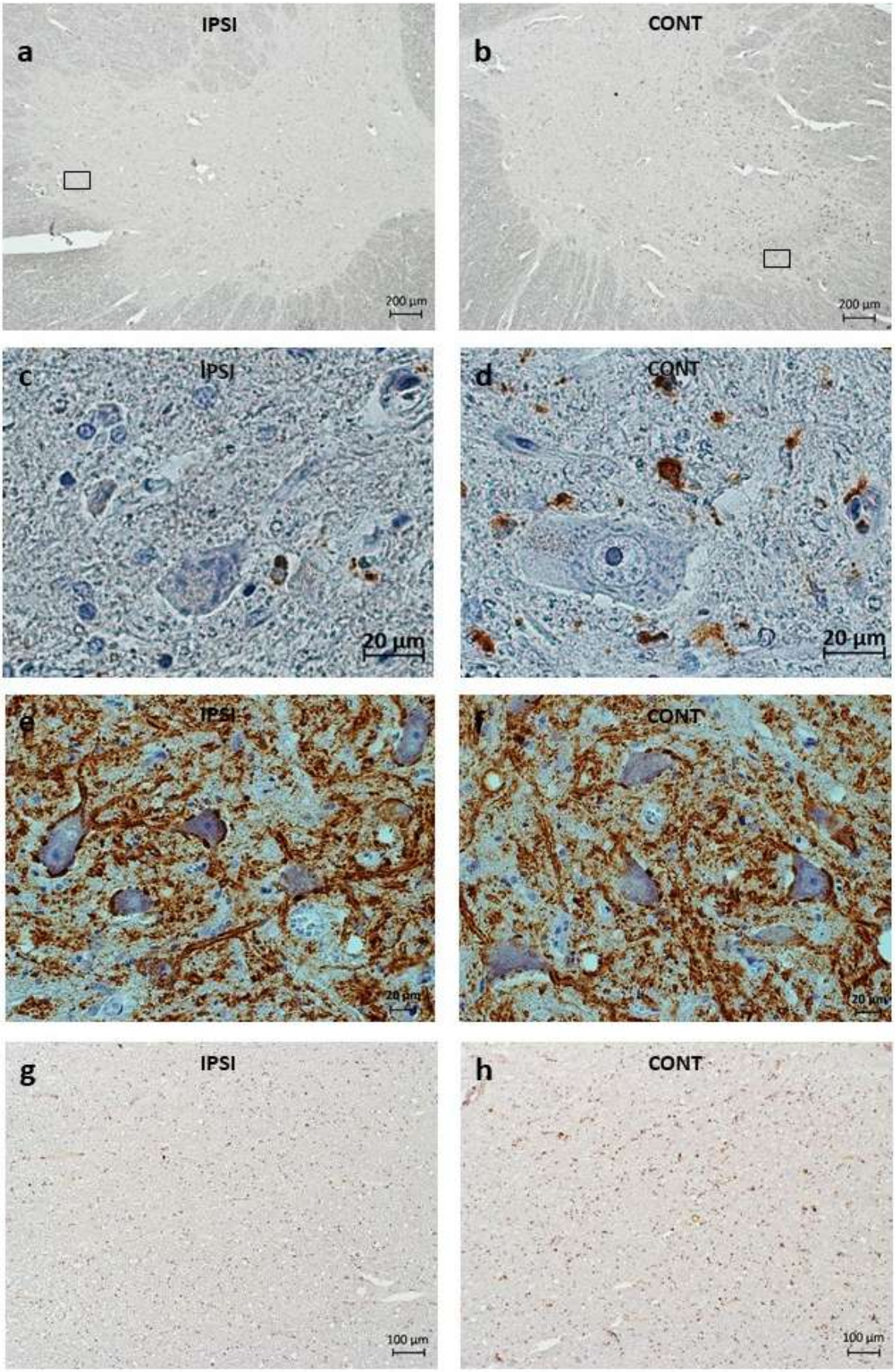
a
IPSI
200 µm
b
CONT
200 µm
c
IPSI
20 µm
d
CONT
20 µm
e
IPSI
f
CONT
g
IPSI
100 µm
h
CONT
100 µm

Figure 6. Pathology of the SpC following stroke.

a, b, c, d Microglial cells (dark dots) in the AH on the intact (IPSI) **(a, c)** and on the contralesional (CONT) **(b, d)** side 6 days after MCA occlusion. CD68 immunhistochemistry with hematoxylin counterstaining.

e, f SYP-coverage of the AHC-s on the intact (IPSI) **(e)** and on the contralesional (CONT) **(f)** side 3 days after MCA occlusion. SYP immunohistochemistry with hematoxylin counterstaining.

g, h Microglial cells (dark dots) in the CST on the intact (IPSI) **(g)** and on the contralesional (CONT) **(h)** side 32 days after MCA occlusion. CD68 immunhistochemistry with hematoxylin counterstaining.

5. DISCUSSION

5.1. Microglia activation along the CST

Previous studies on the human SpC have shown that after stroke, pronounced microglial activation can be detected as early as day 3, not only in the ischaemic infarct area, but also caudal to it, in the lateral bundle - in accordance with WD - and even in the spinal grey matter. (89, 111) In our study we have also investigated earlier cases, and found that microglia activation in the brainstem begins as early as the first day, practically within 24 hours, although no statistical difference is observed between the two sides. The clear and statistically significant difference between the pathological and non-pathological side is observed from day 3, when microglia density is clearly and statistically higher on the ipsilateral, (i.e. pathological) side. Since we assume that WD progresses in a rostro-caudal direction, we also expect that neuroinflammation – represented in our study by microglia activation – would also follow the same rosto-caudal pattern, appearing earlier in the brainstem sections. (5, 27) Studies using PET CT to detect microglia also support this observation. (98, 99) However, in our cases, an increase in microglial activation in the brainstem and the cervical section of the SpC becomes evident at the same time. This raises the possibility that, unlike the degenerative process, neuroinflammation along the injured CST does not spread in a rostro-caudal direction, but rather appears simultaneously along its length. In addition close proximity of the structures examined and the fact that we lacked samples from every time point despite our numerous cases from the first two days may also be an explanation.

The above theory is supported by the fact that in the SpC, in addition to the lateral bundle, there is an excess of microglia in the grey matter at practically the same time, already on day 3, which is probably not due to degeneration of the rostro-caudal axons. This was similarly observed in previous studies, in addition to our present study. (89) What is interesting and a new observation in our case is that the appearance of microglia in the grey matter of the SpC is not homogeneous, but more pronounced in the Rexed 9 zone, where the large motor neurons are located. Since CD68 is a lysosomal protein, a marker of microglial phagocytosis, and there is no primary tissue damage in the spinal cord from which the debris should be removed, it would be reasonable to conclude that microglia

may induce secondary synaptic degeneration or reorganization on the motor neurons. (18, 90, 95)

5.2. Temporal dynamics of the WD of the CST

The cases were grouped based on the appearance of microglial activation and pathological characteristics, resulting in uniform pathological patterns within each group.

In the first week (D1-2 and D3-7 groups), consistent with previous pathological studies, no structural abnormalities were observed in either myelin or axons. During this period, most MRI-based studies also showed no abnormalities. (23, 24, 33, 89, 112, 113)

From day 10 onwards (D10–18 group), marked degeneration of the CST was clearly visible, involving both myelin and axons. Regarding axonal degeneration, our observations are in line with previous findings (23) ; however, myelin degradation has generally been described as a later-onset, prolonged process that can still be detected even years later. (24, 114)

A detailed myelin-focused immunohistochemical study examining several myelin proteins (MAG, PLP, MOG) showed the degradation of myelin proteins starting from day 14. At that time, only the breakdown of MAG (myelin-associated glycoprotein) was detected, while the gradual degradation of the other myelin proteins began in the following weeks. (24, 114)

The conventional Klüver–Barrera staining method, which we also used, has typically been applied in previous neuropathological studies only in much later post-stroke cases for examining myelin. Therefore, our results cannot be directly compared with earlier findings. (19, 36)

Following SpC injury, myelin damage has already been observed as early as day 8, a few centimeters distal to the lesion, using conventional staining (Solochrome-cyanine stain). (22) However, due to the different etiology and the fact that these sections were taken very close to the site of injury, direct comparison with our data is limited.

It can be assumed that the initial structural damage to myelin reduces its staining capacity, facilitating dye washout, while the breakdown of most myelin-associated proteins has not yet started. (114-116) Subsequently, myelin degradation in the central nervous system is a prolonged process, which may play a key role in the lack of regeneration. (5)

Since previous human studies investigating WD in the CNS have typically focused on later time points, this new observation cannot be directly compared with earlier results. Based on the spatial and temporal correlations of our pathological data and previous MRI studies, the combination of axonal degeneration and myelin damage may already cause MRI-detectable changes corresponding to WD from the first week onward. (23, 24, 35, 68, 117-121)

In the later period, from week 3 onwards, continuous axonal and myelin loss over the following year has been confirmed by numerous studies. (5, 24)

Our aim was to determine the temporal dynamics of WD in the CNS and to compare the timing of the processes in different etiologies (hemorrhage and infarction). However, it should be emphasized that, in addition to individual variability, these sequential pathological processes may overlap in time and do not always progress uniformly in each phase. (25)

5.3. Comparison of CST WD dynamics in ischaemic and hemorrhagic stroke

We observed no significant differences in the dynamics of axon degeneration between ischemic and hemorrhagic stroke groups. This finding might support early surgical intervention in hemorrhagic strokes, as mechanical compression alone appears sufficient to induce axonal degeneration with dynamics similar to those of cell death. (122-127) No previous human or animal studies are available that similarly compare corticospinal pathway degeneration after ischaemic and hemorrhagic stroke. While minor differences between the groups cannot be ruled out - due to the lack of data across all time points - any substantial divergence remains unlikely.

5.4. Early signs of transsynaptic degeneration in the anterior horn of the SpC

By performing morphometric analysis of anterior horn cells and assessing the quantity and distribution of their synapses, we aimed to investigate whether microglial proliferation has consequences in the SpC gray matter, and whether the results of electrophysiological studies may be correlated with morphological changes of motoneurons.

In agreement with previous human studies, we found that microglial activation becomes pronounced on the contralateral anterior horn from day 3 post-injury. (89, 96) We found, that this activation shows uneven distribution, with a clear preference for Rexed lamina IX, where large alpha motoneurons are located. This topographical pattern suggests that motoneurons may be more severely affected than local interneurons.

Any injury to the CNS is followed by microglia, whose role is partly protective and beneficial by removing tissue debris, but also harmful by causing secondary damage to neurons. (18, 94, 95)

In cases of cerebral infarction, early microglial activation is not restricted to the ischemic area or the descending CST undergoing WD, but is also observed in the anterior horn of the SpC. Since this occurs concurrently with electrophysiological signs of motoneuron dysfunction, it is reasonable to hypothesize that motoneurons or their synaptic networks undergo structural alterations.

The marker we used, CD68, is a lysosomal membrane protein whose expression increases under conditions of enhanced phagocytic activity. (92, 128) Since there is no primary tissue damage in the SpC following stroke which requires clearance of cellular debris, it is plausible to assume that the activated microglia in the anterior horn contribute to secondary synaptic degeneration or possibly synaptic reorganization.

Human electrophysiological studies have described various signs of lower motoneuron impairment following upper motoneuron lesions. The earliest electrophysiological signs can already be detected on the first day after stroke, reflecting motor unit loss in the paretic muscles. This is typically followed by motor unit reorganization. (71-75, 129)

Besides from the second week onward, spontaneous muscle activity appears, which disappear by six months post-stroke. (71)

These consistent electrophysiological findings suggest the presence of trans-synaptic dysfunction, although histological evidence supporting TND remains limited. To date, only two key studies have addressed this issue.

One study found no significant motoneuron loss in the contralateral anterior horn at the C5 segment, even six months or more after stroke. (69) However, this study did report a significant reduction in the average cross-sectional area of the AHCs compared to the intact ipsilesional side.

Another investigation also failed to find a difference in AHC number, though this study has several methodological limitations. The lesion sites varied considerably across the four subjects, and in one case, the stroke involved the PCA, which does not affect the CST. Furthermore, the study examined the L4 spinal segment, whose motoneurons primarily innervate proximal muscles and receive bilateral corticospinal input. These factors that may explain the lack of detectable changes. (70)

According to our findings, the contralateral anterior horn of the spinal cord shows a slight decrease in overall cell size when the entire cell population is analyzed. At one week post-stroke, the whole population appears to contain larger cells, and the proportion of large neurons is increased on the contralesional side. In later time points, we did not observe similar differences: neither the distribution of cell sizes nor the ratio of large to small neurons showed significant alterations.

These results may indicate a transient morphological change, possibly related to neuronal swelling, primarily affecting cells with an area greater than 700 μm^2, i.e., large alpha-motoneurons. This could represent a morphological correlate of the trans-synaptic dysfunction previously identified by electrophysiological studies. (72, 74, 129)

In addition to morphometric analysis, we assessed synaptic density and quantity using immunohistochemical labeling of SYP, a presynaptic vesicle membrane protein. (104) While our aim was to detect changes in overall synaptic density, we did not observe

significant differences between the two sides of the SpC at this early (in the first month) post-stroke time point.

However, when analyzing individual large alpha-motoneurons, we observed a reduction in SYP coverage on their surface, indicating a decreased number of axon terminals and, consequently, reduced synaptic input. These findings suggest that the synaptic connections of AHCs may be involved in some way. This hypothesis requires further confirmation via electron microscopic analysis in future studies.

The transient increase in neuronal cell size observed in our study may reflect a compensatory mechanism in response to reduced or altered synaptic input. Similar mechanisms have been documented in Alzheimer's disease (AD), where hippocampal CA1 neurons in asymptomatic individuals show larger cell sizes compared to those in patients with mild cognitive impairment or Alzheimer-dementia. (130)

After one month, no significant differences were observed between the ipsi- and contralesional sides of the SpC, which is consistent with findings from previous studies. (69, 70)

Interpretation of our study data is limited by the small number of patients included, but the results are strengthened by rigorous patient selection and detailed morphometric analysis. Further validation in larger trials is needed, but these preliminary data already suggest that spinal motoneurons undergo morphological changes in the first month after stroke, and identification of the biochemical factors underlying these changes may be useful in developing future therapeutic interventions.

6. CONCLUSION

1. Microglial activation in the CST in the medulla oblongata and in the lateral tract and anterior horn of the cervical SpC can be detected as early as day 3 as part of WD after haemorrhagic and ischaemic stroke. Its appearance in the anterior horn is not evenly distributed, but mainly affects lamina IX, where the large motoneurons are located. It does not necessarily show a rostrocaudal pattern, although it becomes more pronounced over the first month.

2. Following microglial activation, structural damage to both myelin and axon at the level of the medulla oblongata is observed from day 7-10 post-stroke, a process that is slow and may take several months. Axon degeneration in ischaemic and haemorrhagic stroke follows similar dynamics.

3. In addition to early microglial activation in the anterior horn of the SpC, a structural change of the anterior horn cells is observed. 7 days after the stroke, they are larger and swollen compared to the contralateral side, a phenomenon that mainly affects the large alpha-motoneurons. This is a temporary feature and no such difference was observed afterwards.

4. Examining synapse density, there was no difference between the anterior horns of the two sides, but examining individual motoneurons, the synaptic endings on the surface of each motoneuron were reduced, suggesting secondary damage and reorganization of synapses.

5. Our histological studies provide support for the previous electrophysiological findings, which had already suggested a transneuronal functional impairment of spinal motoneurons.

6. The results of our study may focus attention on secondary changes after stroke such as transsynaptic degeneration and microglial activation, inducing further detailed research. A deeper analysis of these may also identify potential therapeutic targets for neurorehabilitation and neuroprotection in the future.

7. SUMMARY

The aim of this thesis is to investigate the secondary degenerative processes of the central nervous system after cerebrovascular disease, with special emphasis on WD of the CST and TND of spinal motoneurons. In this study, immunohistochemical and morphometric analyses were performed on postmortem human histological samples. Analyses of CST degeneration showed microglial activation as early as day 3 post-stroke, increased over the following 1 month and persisted up to 1 year later. Signs of axon and myelin damage appeared within 7-10 days and gradually worsened. We found no difference in the dynamics of degeneration between ischaemic and haemorrhagic strokes.

Microglial activation also appeared early in the anterior horn of the SpC, especially in the area of the Rexed IX lamina, where the large alpha-motoneurons are located. Based on the decrease in synaptic coverage of large motoneurons and their increase in size observed one week post-injury, it is hypothesized that transneuronal synaptic reorganization or some kind of functional damage might occur in the first month after stroke.

8. REFERENCES

1. Zedde M, Grisendi I, Assenza F, Napoli M, Moratti C, Di Cecco G, et al. Stroke-Induced Secondary Neurodegeneration of the Corticospinal Tract-Time Course and Mechanisms Underlying Signal Changes in Conventional and Advanced Magnetic Resonance Imaging. J Clin Med. 2024;13(7).
2. Yamada K, Patel U, Shrier DA, Tanaka H, Chang JK, Numaguchi Y. MR imaging of CNS tractopathy: wallerian and transneuronal degeneration. AJR Am J Roentgenol. 1998;171(3):813-8.
3. Manuel B. Graeber WFB, Georg W. Kreutzberg. Cellular pathology of the central nervous system. In: David I. Graham PLL, editor. Greenfield's Neuropathology. I. . 7th ed. London: Arnold; 2002. p. 123-92.
4. Waller A. Experiments on the Section of the Glosso-Pharyngeal and Hypoglossal Nerves of the Frog, and Observations of the Alterations Produced Thereby in the Structure of Their Primitive Fibres. Edinb Med Surg J. 1851;76(189):369-76.
5. Vargas ME, Barres BA. Why is Wallerian degeneration in the CNS so slow? Annu Rev Neurosci. 2007;30:153-79.
6. Coleman MP, Freeman MR. Wallerian degeneration, wld(s), and nmnat. Annu Rev Neurosci. 2010;33:245-67.
7. Zhang K, Jiang M, Fang Y. The Drama of Wallerian Degeneration: The Cast, Crew, and Script. Annu Rev Genet. 2021;55:93-113.
8. Chen YJ, Nabavizadeh SA, Vossough A, Kumar S, Loevner LA, Mohan S. Wallerian Degeneration Beyond the Corticospinal Tracts: Conventional and Advanced MRI Findings. J Neuroimaging. 2017;27(3):272-80.
9. Freeman MR. Signaling mechanisms regulating Wallerian degeneration. Curr Opin Neurobiol. 2014;27:224-31.
10. Conforti L, Gilley J, Coleman MP. Wallerian degeneration: an emerging axon death pathway linking injury and disease. Nat Rev Neurosci. 2014;15(6):394-409.
11. Neukomm LJ, Freeman MR. Diverse cellular and molecular modes of axon degeneration. Trends Cell Biol. 2014;24(9):515-23.
12. Friede RL, Martinez AJ. Analysis of axon-sheath relations during early Wallerian degeneration. Brain Res. 1970;19(2):199-212.

13. Fleck JD, Azzarelli B, Biller J. Wallerian degeneration of the corticospinal tract in a middle cerebral artery infarction. J Stroke Cerebrovasc Dis. 2002;11(3-4):201-3.
14. Jacobowitz DM, Cole JT, McDaniel DP, Pollard HB, Watson WD. Microglia activation along the corticospinal tract following traumatic brain injury in the rat: a neuroanatomical study. Brain Res. 2012;1465:80-9.
15. George R, Griffin JW. Delayed macrophage responses and myelin clearance during Wallerian degeneration in the central nervous system: the dorsal radiculotomy model. Exp Neurol. 1994;129(2):225-36.
16. Beirowski B, Adalbert R, Wagner D, Grumme DS, Addicks K, Ribchester RR, et al. The progressive nature of Wallerian degeneration in wild-type and slow Wallerian degeneration (WldS) nerves. BMC Neurosci. 2005;6:6.
17. Malbouisson AM, Ghabriel MN, Allt G. The non-directional pattern of axonal changes in Wallerian degeneration: a computer-aided morphometric analysis. J Anat. 1984;139 (Pt 1)(Pt 1):159-74.
18. Abe N, Nishihara T, Yorozuya T, Tanaka J. Microglia and Macrophages in the Pathological Central and Peripheral Nervous Systems. Cells. 2020;9(9).
19. Matsusue E, Sugihara S, Fujii S, Kinoshita T, Ohama E, Ogawa T. Wallerian degeneration of the corticospinal tracts: postmortem MR-pathologic correlations. Acta Radiol. 2007;48(6):690-4.
20. Wong KM, Babetto E, Beirowski B. Axon degeneration: make the Schwann cell great again. Neural Regen Res. 2017;12(4):518-24.
21. Stoll G, Jander S, Myers RR. Degeneration and regeneration of the peripheral nervous system: from Augustus Waller's observations to neuroinflammation. J Peripher Nerv Syst. 2002;7(1):13-27.
22. Becerra JL, Puckett WR, Hiester ED, Quencer RM, Marcillo AE, Post MJ, et al. MR-pathologic comparisons of wallerian degeneration in spinal cord injury. AJNR Am J Neuroradiol. 1995;16(1):125-33.
23. Buss A, Brook GA, Kakulas B, Martin D, Franzen R, Schoenen J, et al. Gradual loss of myelin and formation of an astrocytic scar during Wallerian degeneration in the human spinal cord. Brain. 2004;127(Pt 1):34-44.

24. Buss A, Pech K, Merkler D, Kakulas BA, Martin D, Schoenen J, et al. Sequential loss of myelin proteins during Wallerian degeneration in the human spinal cord. Brain. 2005;128(Pt 2):356-64.

25. Bignami A, Ralston HJ, 3rd. The cellular reaction to Wallerian degeneration in the central nervous system of the cat. Brain Res. 1969;13(3):444-61.

26. Neumann H, Kotter MR, Franklin RJ. Debris clearance by microglia: an essential link between degeneration and regeneration. Brain. 2009;132(Pt 2):288-95.

27. Venkatasubramanian C, Kleinman JT, Fischbein NJ, Olivot JM, Gean AD, Eyngorn I, et al. Natural history and prognostic value of corticospinal tract Wallerian degeneration in intracerebral hemorrhage. J Am Heart Assoc. 2013;2(4):e000090.

28. Huisman TA. Diffusion-weighted and diffusion tensor imaging of the brain, made easy. Cancer Imaging. 2010;10 Spec no A(1a):S163-71.

29. Werring DJ, Toosy AT, Clark CA, Parker GJ, Barker GJ, Miller DH, et al. Diffusion tensor imaging can detect and quantify corticospinal tract degeneration after stroke. J Neurol Neurosurg Psychiatry. 2000;69(2):269-72.

30. Puig J, Pedraza S, Blasco G, Daunis IEJ, Prats A, Prados F, et al. Wallerian degeneration in the corticospinal tract evaluated by diffusion tensor imaging correlates with motor deficit 30 days after middle cerebral artery ischemic stroke. AJNR Am J Neuroradiol. 2010;31(7):1324-30.

31. Yu C, Zhu C, Zhang Y, Chen H, Qin W, Wang M, et al. A longitudinal diffusion tensor imaging study on Wallerian degeneration of corticospinal tract after motor pathway stroke. Neuroimage. 2009;47(2):451-8.

32. Soares JM, Marques P, Alves V, Sousa N. A hitchhiker's guide to diffusion tensor imaging. Front Neurosci. 2013;7:31.

33. Domi T, deVeber G, Shroff M, Kouzmitcheva E, MacGregor DL, Kirton A. Corticospinal tract pre-wallerian degeneration: a novel outcome predictor for pediatric stroke on acute MRI. Stroke. 2009;40(3):780-7.

34. Liang Z, Zeng J, Zhang C, Liu S, Ling X, Xu A, et al. Longitudinal investigations on the anterograde and retrograde degeneration in the pyramidal tract following pontine infarction with diffusion tensor imaging. Cerebrovasc Dis. 2008;25(3):209-16.

35. Uchino A, Sawada A, Takase Y, Egashira R, Kudo S. Transient detection of early wallerian degeneration on diffusion-weighted MRI after an acute cerebrovascular accident. Neuroradiology. 2004;46(3):183-8.
36. Jones KC, Hawkins C, Armstrong D, Deveber G, Macgregor D, Moharir M, et al. Association between radiographic Wallerian degeneration and neuropathological changes post childhood stroke. Dev Med Child Neurol. 2013;55(2):173-7.
37. Inoue Y, Matsumura Y, Fukuda T, Nemoto Y, Shirahata N, Suzuki T, et al. MR imaging of Wallerian degeneration in the brainstem: temporal relationships. AJNR Am J Neuroradiol. 1990;11(5):897-902.
38. Tian R, Zhou Y, Ren Y, Zhang Y, Tang W. Wallerian degeneration: From mechanism to disease to imaging. Heliyon. 2025;11(1):e40729.
39. Kuhn MJ, Mikulis DJ, Ayoub DM, Kosofsky BE, Davis KR, Taveras JM. Wallerian degeneration after cerebral infarction: evaluation with sequential MR imaging. Radiology. 1989;172(1):179-82.
40. Forbrig R, Danek A. Wallerian Degeneration of the Pyramidal Tract. Dtsch Arztebl Int. 2022;119(9):141.
41. Puig J, Blasco G, Daunis IEJ, Thomalla G, Castellanos M, Figueras J, et al. Decreased corticospinal tract fractional anisotropy predicts long-term motor outcome after stroke. Stroke. 2013;44(7):2016-8.
42. Bigourdan A, Munsch F, Coupé P, Guttmann CR, Sagnier S, Renou P, et al. Early Fiber Number Ratio Is a Surrogate of Corticospinal Tract Integrity and Predicts Motor Recovery After Stroke. Stroke. 2016;47(4):1053-9.
43. Thomalla G, Glauche V, Koch MA, Beaulieu C, Weiller C, Röther J. Diffusion tensor imaging detects early Wallerian degeneration of the pyramidal tract after ischemic stroke. Neuroimage. 2004;22(4):1767-74.
44. You M, Rong R, Zeng Z, Xia X, Ji D. Transneuronal Degeneration in the Brain During Glaucoma. Front Aging Neurosci. 2021;13:643685.
45. Rossiter JP. Trans-synaptic degeneration of lateral geniculate nuclei following remote loss of right eye. JAMA Ophthalmol. 2015;133(1):e141789.
46. Jindahra P, Petrie A, Plant GT. Retrograde trans-synaptic retinal ganglion cell loss identified by optical coherence tomography. Brain. 2009;132(Pt 3):628-34.

47. Vrabec JP, Levin LA. The neurobiology of cell death in glaucoma. Eye (Lond). 2007;21 Suppl 1:S11-4.

48. Lawlor M, Danesh-Meyer H, Levin LA, Davagnanam I, De Vita E, Plant GT. Glaucoma and the brain: Trans-synaptic degeneration, structural change, and implications for neuroprotection. Surv Ophthalmol. 2018;63(3):296-306.

49. Tur C, Goodkin O, Altmann DR, Jenkins TM, Miszkiel K, Mirigliani A, et al. Longitudinal evidence for anterograde trans-synaptic degeneration after optic neuritis. Brain. 2016;139(Pt 3):816-28.

50. Millington RS, Yasuda CL, Jindahra P, Jenkinson M, Barbur JL, Kennard C, et al. Quantifying the pattern of optic tract degeneration in human hemianopia. J Neurol Neurosurg Psychiatry. 2014;85(4):379-86.

51. Cowey A, Alexander I, Stoerig P. Transneuronal retrograde degeneration of retinal ganglion cells and optic tract in hemianopic monkeys and humans. Brain. 2011;134(Pt 7):2149-57.

52. Park HY, Park YG, Cho AH, Park CK. Transneuronal retrograde degeneration of the retinal ganglion cells in patients with cerebral infarction. Ophthalmology. 2013;120(6):1292-9.

53. Kodama F, Ogawa T, Sugihara S, Kamba M, Kohaya N, Kondo S, et al. Transneuronal degeneration in patients with temporal lobe epilepsy: evaluation by MR imaging. Eur Radiol. 2003;13(9):2180-5.

54. Uchino A, Sawada A, Takase Y, Nomiyama K, Egashira R, Kudo S. Ipsilateral mamillary body atrophy after infarction of the posterior cerebral artery territory: MR imaging. Eur Radiol. 2005;15(11):2312-5.

55. Nakane M, Teraoka A, Asato R, Tamura A. Degeneration of the ipsilateral substantia nigra following cerebral infarction in the striatum. Stroke. 1992;23(3):328-32.

56. Koo MW, Kim YK, Ku KM, Park WW, Minn YK. Exofocal anterograde transsynaptic neuronal death in the globus pallidus: two case reports. J Clin Neurol. 2012;8(4):308-10.

57. Tamura A, Tahira Y, Nagashima H, Kirino T, Gotoh O, Hojo S, et al. Thalamic atrophy following cerebral infarction in the territory of the middle cerebral artery. Stroke. 1991;22(5):615-8.

58. Yamauchi H, Kagawa S, Kusano K, Ito M, Okuyama C. Neuronal Alterations in Secondary Thalamic Degeneration Due to Cerebral Infarction: A (11)C-Flumazenil Positron Emission Tomography Study. Stroke. 2022;53(10):3153-63.
59. Nakane M, Tamura A, Sasaki Y, Teraoka A. MRI of secondary changes in the thalamus following a cerebral infarct. Neuroradiology. 2002;44(11):915-20.
60. Smith MC. Histological findings after hemicerebellectomy in man: anterograde, retrograde and transneuronal degeneration. Brain Res. 1975;95(2-3):423-42.
61. Tien RD, Ashdown BC. Crossed cerebellar diaschisis and crossed cerebellar atrophy: correlation of MR findings, clinical symptoms, and supratentorial diseases in 26 patients. AJR Am J Roentgenol. 1992;158(5):1155-9.
62. Kim JS, Kim SH, Lim SH, Im S, Hong BY, Oh J, et al. Degeneration of the Inferior Cerebellar Peduncle After Middle Cerebral Artery Stroke: Another Perspective on Crossed Cerebellar Diaschisis. Stroke. 2019;50(10):2700-7.
63. Van Eetvelde R, Lemmerling M, Backaert T, Favoreel N, Geerts B, Sommeling C, et al. Imaging Features of Hypertrophic Olivary Degeneration. J Belg Soc Radiol. 2016;100(1):71.
64. Marrakchi S, Hsain IH, Guelzim Y, Ech-Cherif NEK, Fikri M, Jiddane M, et al. Hypertrophic olivary degeneration secondary to a Guillain Mollaret triangle cavernoma: Two case report. Radiol Case Rep. 2024;19(8):3538-44.
65. Bjugn R, Nyengaard JR, Rosland JH. Spinal Cord Transection-No Loss of Distal Ventral Horn Neurons. Exp Neurol. 1997;148(1):179-86.
66. Eidelberg E, Nguyen LH, Polich R, Walden JG. Transsynaptic degeneration of motoneurones caudal to spinal cord lesions. Brain Res Bull. 1989;22(1):39-45.
67. McBride RL, Feringa ER. Ventral horn motoneurons 10, 20 and 52 weeks after T-9 spinal cord transection. Brain Res Bull. 1992;28(1):57-60.
68. Dang G, Chen X, Chen Y, Zhao Y, Ouyang F, Zeng J. Dynamic secondary degeneration in the spinal cord and ventral root after a focal cerebral infarction among hypertensive rats. Sci Rep. 2016;6:22655.
69. Qiu Y, Wada Y, Otomo E, Tsukagoshi H. Morphometric study of cervical anterior horn cells and pyramidal tracts in medulla oblongata and the spinal cord in patients with cerebrovascular diseases. J Neurol Sci. 1991;102(2):137-43.

70. Terao S, Li M, Hashizume Y, Osano Y, Mitsuma T, Sobue G. Upper motor neuron lesions in stroke patients do not induce anterograde transneuronal degeneration in spinal anterior horn cells. Stroke. 1997;28(12):2553-6.

71. McComas AJ, Sica RE, Upton AR, Aguilera N. Functional changes in motoneurones of hemiparetic patients. J Neurol Neurosurg Psychiatry. 1973;36(2):183-93.

72. Arasaki K, Igarashi O, Ichikawa Y, Machida T, Shirozu I, Hyodo A, et al. Reduction in the motor unit number estimate (MUNE) after cerebral infarction. J Neurol Sci. 2006;250(1-2):27-32.

73. Hara Y, Masakado Y, Chino N. The physiological functional loss of single thenar motor units in the stroke patients: when does it occur? Does it progress? Clin Neurophysiol. 2004;115(1):97-103.

74. Lukács M, Vécsei L, Beniczky S. Changes in muscle fiber density following a stroke. Clin Neurophysiol. 2009;120(8):1539-42.

75. Tang W, Zhang X, Tang X, Cao S, Gao X, Chen X. Surface Electromyographic Examination of Poststroke Neuromuscular Changes in Proximal and Distal Muscles Using Clustering Index Analysis. Front Neurol. 2017;8:731.

76. McComas AJ, Fawcett PR, Campbell MJ, Sica RE. Electrophysiological estimation of the number of motor units within a human muscle. J Neurol Neurosurg Psychiatry. 1971;34(2):121-31.

77. Lukács M. Electrophysiological signs of changes in motor units after ischaemic stroke. Clin Neurophysiol. 2005;116(7):1566-70.

78. Selvan VA. Single-fiber EMG: A review. Ann Indian Acad Neurol. 2011;14(1):64-7.

79. Chang CW. Evident transsynaptic degeneration of motor neurons after spinal cord injury: a study of neuromuscular jitter by axonal microstimulation. Am J Phys Med Rehabil. 1998;77(2):118-21.

80. Cruz Martínez A, del Campo F, Mingo MR, Pérez Conde MC. Altered motor unit architecture in hemiparetic patients. A single fibre EMG study. J Neurol Neurosurg Psychiatry. 1982;45(8):756-7.

81. Uesugi H, Sonoo M, Stålberg E, Matsumoto K, Higashihara M, Murashima H, et al. "Clustering Index method": a new technique for differentiation between neurogenic and myopathic changes using surface EMG. Clin Neurophysiol. 2011;122(5):1032-41.
82. Stålberg E, van Dijk H, Falck B, Kimura J, Neuwirth C, Pitt M, et al. Standards for quantification of EMG and neurography. Clin Neurophysiol. 2019;130(9):1688-729.
83. Li Q, Barres BA. Microglia and macrophages in brain homeostasis and disease. Nat Rev Immunol. 2018;18(4):225-42.
84. Woodburn SC, Bollinger JL, Wohleb ES. The semantics of microglia activation: neuroinflammation, homeostasis, and stress. J Neuroinflammation. 2021;18(1):258.
85. Garaschuk O, Verkhratsky A. Physiology of Microglia. Methods Mol Biol. 2019;2034:27-40.
86. Loane DJ, Kumar A. Microglia in the TBI brain: The good, the bad, and the dysregulated. Exp Neurol. 2016;275 Pt 3(0 3):316-27.
87. Perry VH, O'Connor V. The role of microglia in synaptic stripping and synaptic degeneration: a revised perspective. ASN Neuro. 2010;2(5):e00047.
88. Estes ML, McAllister AK. Alterations in immune cells and mediators in the brain: it's not always neuroinflammation! Brain Pathol. 2014;24(6):623-30.
89. Schmitt AB, Buss A, Breuer S, Brook GA, Pech K, Martin D, et al. Major histocompatibility complex class II expression by activated microglia caudal to lesions of descending tracts in the human spinal cord is not associated with a T cell response. Acta Neuropathol. 2000;100(5):528-36.
90. Minett T, Classey J, Matthews FE, Fahrenhold M, Taga M, Brayne C, et al. Microglial immunophenotype in dementia with Alzheimer's pathology. J Neuroinflammation. 2016;13(1):135.
91. Douglas GW. Defining activation states of microglia in human brain tissue: an unresolved issue for Alzheimer's disease. Neuroimmunology and Neuroinflammation. 2020;7(3):194-214.
92. Chistiakov DA, Killingsworth MC, Myasoedova VA, Orekhov AN, Bobryshev YV. CD68/macrosialin: not just a histochemical marker. Lab Invest. 2017;97(1):4-13.
93. Waller R, Baxter L, Fillingham DJ, Coelho S, Pozo JM, Mozumder M, et al. Iba-1-/CD68+ microglia are a prominent feature of age-associated deep subcortical white matter lesions. PLoS One. 2019;14(1):e0210888.

94. Block F, Dihné M, Loos M. Inflammation in areas of remote changes following focal brain lesion. Prog Neurobiol. 2005;75(5):342-65.
95. Jassam YN, Izzy S, Whalen M, McGavern DB, El Khoury J. Neuroimmunology of Traumatic Brain Injury: Time for a Paradigm Shift. Neuron. 2017;95(6):1246-65.
96. Schmitt AB, Brook GA, Buss A, Nacimiento W, Noth J, Kreutzberg GW. Dynamics of microglial activation in the spinal cord after cerebral infarction are revealed by expression of MHC class II antigen. Neuropathol Appl Neurobiol. 1998;24(3):167-76.
97. Gerhard A, Schwarz J, Myers R, Wise R, Banati RB. Evolution of microglial activation in patients after ischemic stroke: a [11C](R)-PK11195 PET study. Neuroimage. 2005;24(2):591-5.
98. Thiel A, Radlinska BA, Paquette C, Sidel M, Soucy JP, Schirrmacher R, et al. The temporal dynamics of poststroke neuroinflammation: a longitudinal diffusion tensor imaging-guided PET study with 11C-PK11195 in acute subcortical stroke. J Nucl Med. 2010;51(9):1404-12.
99. Ghosh SK, Walocha JA. Evolution of staining methods in neuroanatomy: Impetus for emanation of neuron doctrine during the turn of 20th century. Anat Rec (Hoboken). 2024;307(10):3398-412.
100. Kluver H, Barrera E. A method for the combined staining of cells and fibers in the nervous system. J Neuropathol Exp Neurol. 1953;12(4):400-3.
101. Bolon B, Moser A, Chlipala E. Myelin Methods: A Mini-Review. Toxicol Pathol. 2025;53(4):345-54.
102. Ramos-Vara JA. Technical aspects of immunohistochemistry. Vet Pathol. 2005;42(4):405-26.
103. Kim SW, Roh J, Park CS. Immunohistochemistry for Pathologists: Protocols, Pitfalls, and Tips. J Pathol Transl Med. 2016;50(6):411-8.
104. Thiel G. Synapsin I, synapsin II, and synaptophysin: marker proteins of synaptic vesicles. Brain Pathol. 1993;3(1):87-95.
105. Wiedenmann B, Franke WW. Identification and localization of synaptophysin, an integral membrane glycoprotein of Mr 38,000 characteristic of presynaptic vesicles. Cell. 1985;41(3):1017-28.

106. Park D, Wu Y, Lee SE, Kim G, Jeong S, Milovanovic D, et al. Cooperative function of synaptophysin and synapsin in the generation of synaptic vesicle-like clusters in non-neuronal cells. Nat Commun. 2021;12(1):263.
107. Yuan A, Rao MV, Veeranna, Nixon RA. Neurofilaments at a glance. J Cell Sci. 2012;125(Pt 14):3257-63.
108. Gafson AR, Barthélemy NR, Bomont P, Carare RO, Durham HD, Julien JP, et al. Neurofilaments: neurobiological foundations for biomarker applications. Brain. 2020;143(7):1975-98.
109. Lovas G, Szilágyi N, Majtényi K, Palkovits M, Komoly S. Axonal changes in chronic demyelinated cervical spinal cord plaques. Brain. 2000;123 (Pt 2):308-17.
110. Jean Shoenen RLMF. Spinal Cord: Cyto- and Chemoarchitecture. In: Paxinos G MJ, editor. The Human Nervous System. 2nd ed: Elsevier Academic Press; 2004. p. 190-232.
111. Kösel S, Egensperger R, Bise K, Arbogast S, Mehraein P, Graeber MB. Long-lasting perivascular accumulation of major histocompatibility complex class II-positive lipophages in the spinal cord of stroke patients: possible relevance for the immune privilege of the brain. Acta Neuropathol. 1997;94(6):532-8.
112. Kirton A, Shroff M, Visvanathan T, deVeber G. Quantified corticospinal tract diffusion restriction predicts neonatal stroke outcome. Stroke. 2007;38(3):974-80.
113. Koyama T, Uchiyama Y, Domen K. Associations of Diffusion-Tensor Fractional Anisotropy and FIM Outcome Assessments After Intracerebral Hemorrhage. J Stroke Cerebrovasc Dis. 2018;27(10):2869-76.
114. Kister A, Kister I. Overview of myelin, major myelin lipids, and myelin-associated proteins. Front Chem. 2022;10:1041961.
115. García-García Ó D, Carriel V, Chato-Astrain J. Myelin histology: a key tool in nervous system research. Neural Regen Res. 2024;19(2):277-81.
116. Stoll G, Müller HW. Nerve injury, axonal degeneration and neural regeneration: basic insights. Brain Pathol. 1999;9(2):313-25.
117. DeVetten G, Coutts SB, Hill MD, Goyal M, Eesa M, O'Brien B, et al. Acute corticospinal tract Wallerian degeneration is associated with stroke outcome. Stroke. 2010;41(4):751-6.

118. Lama S, Qiao M, Kirton A, Sun S, Cheng E, Foniok T, et al. Imaging corticospinal degeneration in neonatal rats with unilateral cerebral infarction. Exp Neurol. 2011;228(2):192-9.
119. Møller M, Frandsen J, Andersen G, Gjedde A, Vestergaard-Poulsen P, Østergaard L. Dynamic changes in corticospinal tracts after stroke detected by fibretracking. J Neurol Neurosurg Psychiatry. 2007;78(6):587-92.
120. Ni J, Li ML, Yao M, Cui LY. Early corticospinal tract Wallerian degeneration on diffusion-weighted MR imaging after adult stroke: three cases report. Clin Neurol Neurosurg. 2013;115(7):1164-6.
121. Yu X, Jiaerken Y, Wang S, Hong H, Jackson A, Yuan L, et al. Changes in the Corticospinal Tract Beyond the Ischemic Lesion Following Acute Hemispheric Stroke: A Diffusion Kurtosis Imaging Study. J Magn Reson Imaging. 2020;52(2):512-9.
122. Fischer U, Fung C, Beyeler S, Bütikofer L, Z'Graggen W, Ringel F, et al. Swiss trial of decompressive craniectomy versus best medical treatment of spontaneous supratentorial intracerebral haemorrhage (SWITCH): an international, multicentre, randomised-controlled, two-arm, assessor-blinded trial. Eur Stroke J. 2024:23969873241231047.
123. Greenberg SM, Ziai WC, Cordonnier C, Dowlatshahi D, Francis B, Goldstein JN, et al. 2022 Guideline for the Management of Patients With Spontaneous Intracerebral Hemorrhage: A Guideline From the American Heart Association/American Stroke Association. Stroke. 2022;53(7):e282-e361.
124. Hadjiathanasiou A, Schuss P, Ilic I, Borger V, Vatter H, Güresir E. Decompressive craniectomy for intracerebral haematoma: the influence of additional haematoma evacuation. Neurosurg Rev. 2018;41(2):649-54.
125. Kapapa T, Jesuthasan S, Schiller F, Schiller F, Oehmichen M, Woischneck D, et al. Outcome after Intracerebral Haemorrhage and Decompressive Craniectomy in Older Adults. Neurol Int. 2024;16(3):590-604.
126. Marinkovic I, Strbian D, Pedrono E, Vekovischeva OY, Shekhar S, Durukan A, et al. Decompressive craniectomy for intracerebral hemorrhage. Neurosurgery. 2009;65(4):780-6, 1 p following 6; discussion 6.

127. Vahedi K, Hofmeijer J, Juettler E, Vicaut E, George B, Algra A, et al. Early decompressive surgery in malignant infarction of the middle cerebral artery: a pooled analysis of three randomised controlled trials. Lancet Neurol. 2007;6(3):215-22.
128. Henstridge CM, Tzioras M, Paolicelli RC. Glial Contribution to Excitatory and Inhibitory Synapse Loss in Neurodegeneration. Front Cell Neurosci. 2019;13:63.
129. Lukács M, Vécsei L, Beniczky S. Large motor units are selectively affected following a stroke. Clin Neurophysiol. 2008;119(11):2555-8.
130. Iacono D, Markesbery WR, Gross M, Pletnikova O, Rudow G, Zandi P, et al. The Nun study: clinically silent AD, neuronal hypertrophy, and linguistic skills in early life. Neurology. 2009;73(9):665-73.

9. BIBLIOGRAPGY OF THE CANDIDATE'S PUBLICATIONS

Publications related to the subject of the dissertation:

Kollai, S. ; Bereczki, D. ; Glasz, T. ; Hortobágyi, Tibor ; Kovács, T. Early histopathological changes of secondary degeneration in the spinal cord after total MCA territory stroke SCIENTIFIC REPORTS 13 : 1 Paper: 21934 , 9 p. (2023) DOI: 10.1038/s41598-023-49230-x

Kollai, S. ; Bereczki, D. ; Dobi, B. ; Glasz, T. ; Kovács, T. Histopathological Changes of the Corticospinal Tract Following Hemorrhagic and Ischemic Stroke BRAIN SCIENCES 15 : 8 p. 864 (2025) DOI: 10.3390/brainsci15080864

Other publications:

Varga, G ✉ ; Mikala, G ; Gopcsa, L ; Csukly, Z ; Kollai, S ; Balázs, G ; Timár, B ; Wohner, N ; Horváth, L ; Szombath, G et al. Multiple Myeloma of the Central Nervous System: 13 Cases and Review of the Literature JOURNAL OF ONCOLOGY 2018 Paper: 3970169 , 7 p. (2018) DOI: 10.1155/2018/3970169

10. ACKNOWLEDGEMENTS

I would like to express my sincere gratitude to my supervisor, Dr. Tibor Kovács, for his professional support, patience, helpfulness, and guidance throughout the entire process of my research and the preparation of this dissertation.

I am also deeply grateful to Professor Dr. Dániel Bereczki, Head of the Institute, who provided me with the opportunity to carry out my research, and whose patience and commitment to creating a supportive environment greatly contributed to my professional development.

I would like to thank my close colleagues as well, who offered me both professional and personal support, and whose encouraging attitude motivated me the entire time.

Finally, I owe special thanks to the histology assistants, Eszter and Zsuzsi, who, in addition to preparing countless sections, were always very helpful with any practical issues that arose.